Cold Regions Science and Technology 204 (2022) 103663

Contents lists available at ScienceDirect

Cold Regions Science and Technology

journal homepage: www.elsevier.com/locate/coldregions

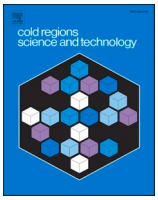

Ice conditions in northern Norwegian fjords: Observations and measurements from three winter seasons, 2017–2020

Megan O'Sadnick [a,b,*], Chris Petrich [b], Camilla Brekke [a], Jofrid Skarðhamar [c], Øystein Kleven [b]

[a] UiT The Arctic University of Norway, Tromsø, Norway
[b] SINTEF Narvik, Narvik, Norway
[c] Institute of Marine Research, Tromsø, Norway

ARTICLE INFO

Keywords:
Sea ice
Fjords
Ice-ocean interaction
Coastal processes

ABSTRACT

Freshwater provided by rivers beginning deep within the mountains, feeds into fjords along the coast of Norway, often forming a brackish surface layer that will change in its salinity, thickness, and extent throughout the year. As temperature drops below freezing, ice can form from this layer along the entire coastline from 71° N down to 58° N. The influence of freshwater combined with changing weather and oceanographic conditions, can lead to ice that varies not only in its thickness and extent but its properties including crystal fabric, bulk salinity, and pore structure. Resultantly, how ice interacts with the surrounding environment including communities that use the ice for winter activities, boats transiting through fjords, pollutants like oil, and the biota living within the ice and fjord waters, will be impacted.

To enhance understanding of the drivers of ice formation and resultant properties in Norwegian fjords, seven fjords located in northern Norway were monitored over three winter seasons between 2017 and 2020. Measurements of ice thickness, stratigraphy, bulk salinity, and $\delta^{18}O$ were gathered along with measurements of ocean salinity, temperature, and $\delta^{18}O$ of both snow and river water. Ice thickness ranged from non-existent up to 0.8 m with the proportion of congelation to granular ice changing between seasons and fjords. While ocean salinities directly below the ice on the day of measurement were primarily above 31 psu, ice bulk salinity varied from 0 psu to 5.6 psu with values of $\delta^{18}O$ between −13.3 ‰ and 0.2 ‰, indicating ice frozen from fresh water as well as seawater. Findings support that ice conditions in a single fjord or in a geographic region should not be generalized, with substantial variations measured between years and locations. We examine openly accessible interpolated weather and runoff data obtained through seNorge for possible causes for the variable ice conditions observed. Results reveal freezing degree days are not a dependable predictor of ice thickness when applied to Norwegian fjords, and substantial consideration of the date of onset of ice formation and snow cover are needed. Freshwater runoff and snowfall as well as the timing of weather and oceanic conditions throughout the three winter seasons are also presented to highlight their potential to influence ice formation considerably.

1. Introduction

The coast of mainland Norway is dominated by the presence of fjords cutting into the adjacent mountains, with the glaciers that carved these fjords now receded into higher terrain if not gone entirely (Holtedahl, 1967; Porter, 1989). Fjords differ in width, length, depth, and orientation with these characteristics transferring to the physical and biological characteristics of fjords including weather, oceanography, and the plants and biota present (Eilertsen and Skarðhamar, 2006; Rikardsen et al., 2004). Often subjected to temperatures below freezing, fjords have the possibility to form ice. While the Norwegian pilot guide offers brief descriptions of ice conditions in selected areas to assist boat and ship captains (Hughes, 2006), no studies exist that make direct observations of sea ice thickness, extent and properties in fjords found throughout mainland Norway. Ice conditions in the pilot guide are themselves based primarily off aging data published in older editions mixed with examination of visible and infrared satellite images gathered in February and March 2005.

The larger fjords along the Norwegian coast are ice free all year due to the influence of warm Atlantic water (Aure et al., 1996; Eilertsen and Skarðhamar, 2006). However, sea ice often forms in the inner parts of fjords and in smaller fjord branches (O'Sadnick et al., 2020). There is a

* Corresponding author at: UiT The Arctic University of Norway, Tromsø, Norway.
E-mail address: megan.osadnick@sintef.no (M. O'Sadnick).

https://doi.org/10.1016/j.coldregions.2022.103663
Received 28 May 2021; Received in revised form 5 August 2022; Accepted 23 August 2022
Available online 31 August 2022

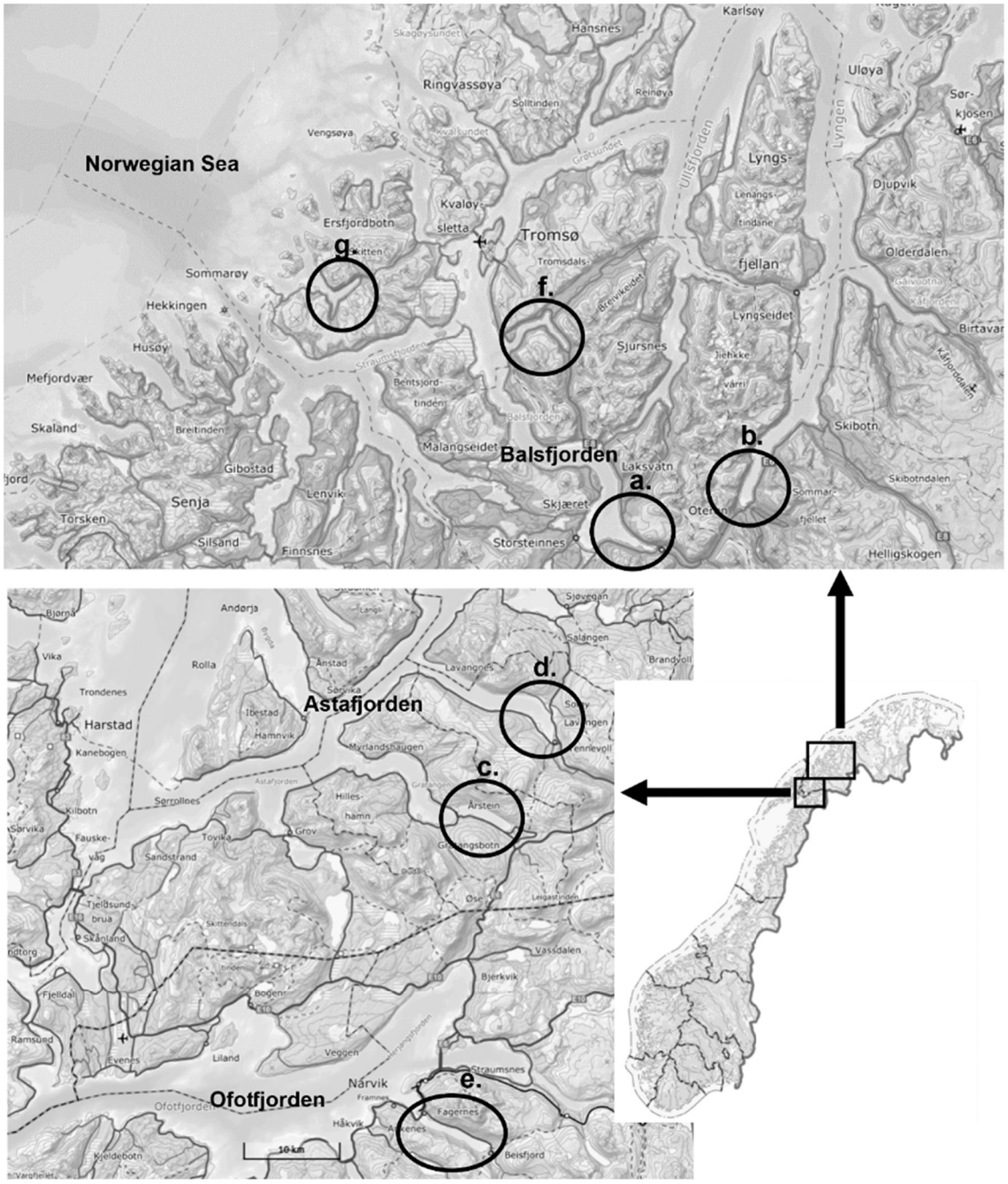

Fig. 1. Location of Norwegian fjords where measurements were gathered, ordered according to freezing degree days (FDD) from highest to lowest. a) Nordkjosbotn, b) Storfjord, c) Gratangsbotn, d) Lavangen, e) Beisfjord, f) Ramfjord, g) Kattfjord. ©norgeskart.no.

wide breadth of work in mainland Norwegian fjords focusing on water mass dynamics, often linked to biological processes in open waters (Asplin et al., 1999; Cottier et al., 2010; Eilertsen and Skarðhamar, 2006; Jones et al., 2020; Mankettikkara, 2013; Skarðhamar et al., 2018). However, little research has so far been conducted on sea ice in Norwegian fjords (O'Sadnick et al., 2020), while the role of sea ice in fjords on Svalbard is well studied (for example Cottier et al., 2010; Gerland and Renner, 2007; Hop and Wiencke, 2019; Nilsen et al., 2008; Skogseth et al., 2020).

When ice forms on the surface of a fjord, it creates a barrier between the ocean and air, altering the exchange of mass and energy (Petrich and Eicken, 2010). In addition, ice creates a biologically rich environment of brine-filled pores that offer a sheltered place for algae and other microbiota to grow (Arrigo et al., 2010; Brandon et al., 2010; Gradinger et al., 1999). Studies of sea ice in the Baltic Sea offer descriptions of ice grown from sea water of lower salinity, brackish in character, as well as the impact of fresh water plumes on local ecology (Granskog et al., 2005a; Granskog et al., 2005b; Kaartokallio et al., 2007). However, these studies may be difficult to apply to fjord ice where a stratified water column is often observed characterized by a surface layer that is reduced in salinity due to freshwater, an intermediary layer similar in composition to coastal water, and a basin holding the densest water below the depth of a sill (Stigebrandt, 2012). Fjords are also well contained by coastline and bed topography impacting currents and fjord-coast water exchange.

Though little work is available documenting observations of specifically Norwegian fjords in winter (Walker et al., 2021; Eilertsen and Skarðhamar, 2006), research focused on the more general field of Arctic

Table 1
Overview of ice conditions in the fjords. Dates of formation of consistent ice cover and when the fjords were ice free are from observations with cameras and/or satellite imagery.

Season	Ice formation	Ice free	Date of meas.	Fraction of season complete at meas.	Ice thickness [m]	Snow depth [m]	Freeboard [m]
Nordkjosbotn							
2017/18	29–30 Dec	27–30 Apr	20 Mar 2018	81/122	0.76	0.06	n/m
2018/19	29–30 Jan	16–24 Apr	13 Mar 2019	43/76	0.15	n/m	n/m
2019/20	6–8 Mar	16–20 Mar	n/m	−/14	n/m	n/m	n/m
Storfjord							
2017/18	15–20 Feb	20–23 Apr	20 Mar 2018	33/67	0.36	0.10–0.15	n/m
2018/19	n/a	n/a	12 Mar 2019	n/a	n/a	n/a	n/a
2019/20	n/a	n/a	11 Mar 2020	n/a	n/a	n/a	n/a
Gratangsbotn							
2017/18	n/a	n/a	23 Mar 2018	n/a	n/a	n/a	n/a
2018/19	27–29 Jan	16–24 Apr	14 Mar 2019	46/87	0.27	0.21	negative
2019/20	4–10 Dec	22 Apr	20 Feb 2020	78/140	0.21	0.11	negative
Lavangen							
2017/18	27–28 Jan	20–23 Apr	23 Mar 2018	55/86	0.37	0.16	n/m
2018/19	20–23 Jan	16–24 Apr	14 Mar 2019	53/94	0.26	0.02	0.03
2019/20	1–5 Feb	31 Mar - 4 Apr	n/m	−/63	n/m	n/m	n/m
Beisfjord							
2017/18	1–5 Feb	5–11 May	19 Apr 2018	77/99	0.42	0.10	n/m
2018/19	3 Mar	21 Apr	19 Mar 2019	16/49	0.24 (a)/0.235 (b)/ 0.18 (c)/ 0.08 (d)	0.0	0.01
2019/20	9 Dec	20–26 Jan	22 Feb 2020	−/48	n/m	n/m	n/m
Ramfjord							
2017/18	28–29 Jan	5–11 May	20 Mar 2018	51/103	0.49	0.2	n/m
2018/19	20 Dec	7 May	13 Mar 2019	83/138	0.46	n/m	negative
2019/20	15 Oct	24 May	12 Mar 2020	148/222	0.30	0.20	negative
Kattfjord							
2017/18	5–10 Jan	5–11 May	21 Mar 2018	75/126	0.59	0.23	negative
2018/19	14 Jan	26–27 Apr	14 Mar 2019	59/103	0.35	0.37	negative
2019/20	n/a	n/a	12 Mar 2020	n/a	n/a	n/a	n/a

Ice thickness, snow depth and freeboard were measured on the dates given. Gray, shaded entries represent visits where only ocean and fresh water measurements were obtained. When ice was present but no measurement made, the season length in days is provided. n/m = not measured, n/a = no ice.

estuaries does exist from e.g. North America and Russia. Macdonald et al. (1995), Macdonald et al. (1999), and Eicken et al. (2005) attempted to quantify the fraction of ice grown from river discharge in coastal sea ice by examining the isotopic signature of both the ice and the water from which it is grown. The isotopic composition $\delta^{18}O$ is defined as:

$$\delta^{18}\mathrm{O} = \left(\frac{\left(\frac{^{18}O}{^{16}O}\right)_{sample}}{\left(\frac{^{18}O}{^{16}O}\right)_{standard}} - 1 \right) * 1000 \quad (1)$$

where the standard is Vienna Standard Mean Ocean Water (VSMOS).

Similarly to salinity, the stable isotope ratio in ice is sensitive to both

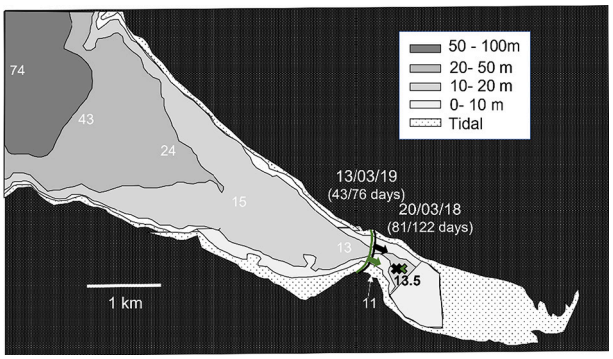

Fig. 2. Nordkjosbotn, in the inner part of Balsfjorden. Water depth in meters marked along the length of the fjord, contours are also shown. Ice extent on the day of measurement (indicated, see text for details) and measurement location are marked with a line across the fjord and a cross, respectively, for seasons 2017/18 (black), and 2018/19 (green). (For interpretation of the references to colour in this figure legend, the reader is referred to the web version of this article.)

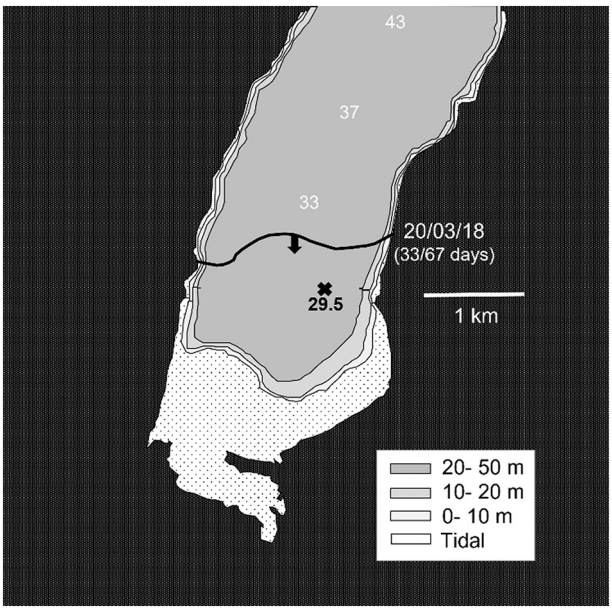

Fig. 3. Storfjord. Water depth in meters marked along the length of the fjord, contours also shown. Ice extent on the day of measurement and measurement location marked with a line across the fjord and a cross, respectively, for the 2017/18 season.

source water and growth rate. For the former, fresh water for example may come from a river, snow melt, or ice melt to mention a few possible sources. A study by Nan et al. (2019), found the isotopic signature of fresh river water to vary across the globe with values in Norway, specifically, ranging from approximately −12‰ in the north up to −4‰ further south. For ocean water, the Vienna Standard has a $\delta^{18}O$ of 0‰ while values as high as approximately 2‰ at lower latitudes down to −3‰ in regions of the arctic have been measured (LeGrande and Schmidt, 2006). Therefore, even if all sources carry the same salinity, $\delta^{18}O$ can differ. Additionally, growth rate will impact values of $\delta^{18}O$. A decrease in growth rate will increase isotopic fractionation (increasing values of $\delta^{18}O$, cf. Eq.1) (Eicken, 1998).The opposite impact is seen in measurements of bulk salinity which decreases in magnitude with a decrease in growth rate.

Through using measurements of $\delta^{18}O$, the above authors were able to trace events of larger freshwater flux during the winter and approximate

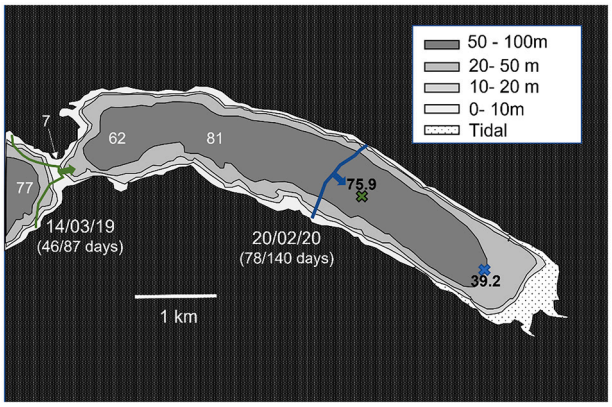

Fig. 4. Gratangsbotn. Water depth in meters marked along the length of the fjord, contours also shown. Ice extent on the day of measurement and measurement location marked with a line across the fjord and a cross, respectively, for seasons, 2018/19 (green), and 2019/20 (blue). (For interpretation of the references to colour in this figure legend, the reader is referred to the web version of this article.)

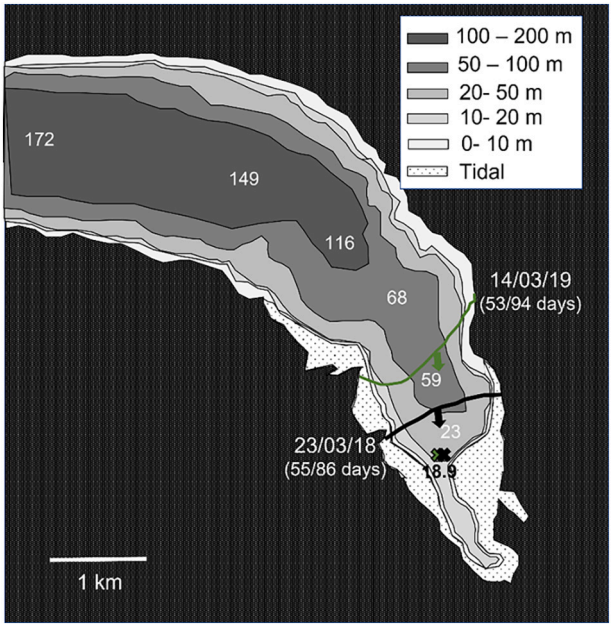

Fig. 5. Lavangen. Water depth in meters marked along the length of the fjord, contours also shown. Ice extent on the day of measurement and measurement location marked with a line across the fjord and a cross, respectively, for seasons 2017/18 (black), 2018/19 (green),. (For interpretation of the references to colour in this figure legend, the reader is referred to the web version of this article.)

the size and movement of freshwater plumes under the ice. The extent of these plumes is important as they disable convection under the ice, diluting and sweeping away brine rejected from the ice and changing the overall oceanographic conditions within the area. Granskog et al. (2005a, 2005b) examine the impact of such plumes in the Baltic Sea, noting that plumes of fresh water can also act to stabilize the water column reducing heat exchange with the ocean and causing faster ice growth.

Freshwater under the ice can lead to the formation of ice layers of low porosity that are essentially impermeable to fluid flow. These layers can disrupt the convection of brine through the ice and the exchange of nutrients that enables the growth of ice-algal communities. Ingram et al. (1996) investigated the impact of freshwater on an ecosystem under sea

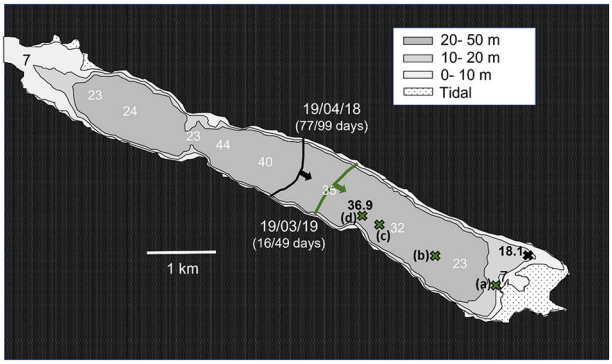

Fig. 6. Beisfjord. Water depth in meters marked along the length of the fjord, contours also shown. Ice extent on the day of measurement and measurement location marked with a line across the fjord and a cross, respectively, for seasons 2017/18 (black), 2018/19 (green). (For interpretation of the references to colour in this figure legend, the reader is referred to the web version of this article.)

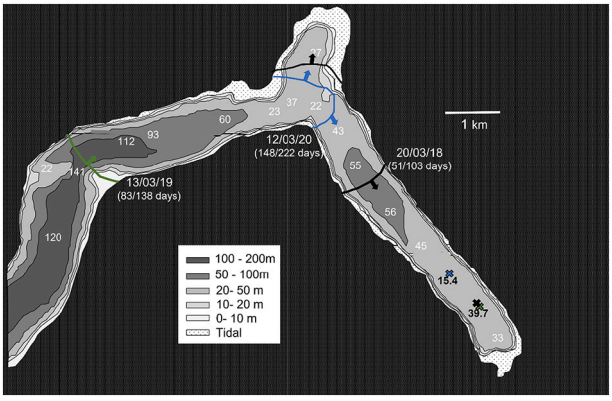

Fig. 7. Ramfjord. Water depth in meters marked along the length of the fjord, contours also shown. Ice extent on the day of measurement and measurement location marked with a line across the fjord and a cross, respectively, for seasons 2017/18 (black), 2018/19 (green), and 2019/20 (blue). (For interpretation of the references to colour in this figure legend, the reader is referred to the web version of this article.)

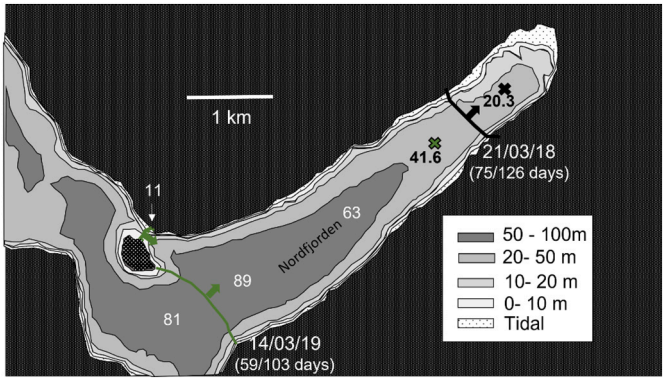

Fig. 8. Kattfjord. Water depth in meters marked along the length of the fjord, contours also shown. Ice extent on the day of measurement and measurement location marked with a line across the fjord and a cross, respectively, for seasons 2017/18 (black) and 2018/19 (green). (For interpretation of the references to colour in this figure legend, the reader is referred to the web version of this article.)

ice through linking the sea water salinity at the ice interface to various environmental and biological response variables including bulk ice salinity, light attenuation, chlorophyll *a*, and algal diversity. The authors stressed the need for further work examining coastal zones in northern areas; placing focus on the impact of freshwater flow on the hydrodynamics and the ecology of an area.

Whether caused by an influx of freshwater or other factors such as changing weather or oceanic conditions, the microstructure of sea ice and the connectivity of pore space are often a focus in scientific studies. While measurements of temperature, bulk salinity, and stable isotopes are useful, visual examination of sea ice thick sections has proven useful in determining the cause of patterns in sea ice microstructure. For example, banding, simply described as the variation in transmittance of light through the ice, can reveal where pore shape and connectivity may change. Cole et al. (2004) studied banding in first year sea ice present in Utqiaġvik (previously Barrow, Alaska) over the course of three seasons. In the Arctic, first year sea ice can be found along much of the coastline. This ice often has a bulk salinity between 5 and 8 (psu) and is distinguished from freshwater ice in crystal structure and the presence of pores holding brine. As the ice warms in spring, these pores connect in the vertical direction allowing for fluid flow through the ice when temperature is above approximately −5 °C. Cole et al. (2004) analyzed the shape and geometry of the pores present in bands of high and low porosity, i.e., light and dark bands respectively. Results provided a first order description and estimate of pore density, structure, and variability. In addition, Turner et al. (2017), examined banding in Antarctic ice focusing primarily on the appearance of thin, recurring bands. They determined that such a pattern is related to the changing boundary layer conditions that result from tidal currents.

Layers of freshwater ice have implications for operations in ice-covered waters. As marine traffic increases in Arctic coastal regions, the risk of an oil spill, either from ships or oil production, is also becoming more of a concern. Previous studies examining the interaction of oil and ice, have focused on sea ice of columnar structure that undergoes a predictable evolution through the ice season. In such ice, oil emplaced under and possibly frozen into the ice, would rise to the surface during spring warming as pores connect and a pathway through the ice to the surface are created (Dickens, 2011; Petrich et al., 2013). If layers of lower porosity or possibly impermeable ice are present, this process will be disrupted resulting in a less predictable and likely more challenging approach to oil clean up. This risk applies not only to Norwegian fjords but any area where freshwater interacts with sea ice during the ice growth period. Additionally, freshwater ice and sea ice have different mechanical properties, a characteristic due largely to the former having greater strength because of lower porosity. A simple explanation isthat fewer pores means there is more “solid ice” within the sample (Timco and Weeks, 2010). Relatedly, ice porosity will alter the electrical signature of the ice impacting how ice is seen by remote sensing instruments (Tucker et al., 1992). All these factors are important for operations in the Arctic and sub-Arctic regions. Therefore, the findings presented here have implications for science and industry including biology, shipping and transit in Arctic and sub-Arctic regions, safety for local communities, and oil spill response methods.

The objective of this study is to investigate the ice conditions and properties in northern Norwegian mainland fjords, and how and why the fjord ice varies between years and between neighboring fjords. We present measurements from seven fjords in northern Norway collected over the span of three winter seasons between 2017 to 2020 combined with openly available weather and runoff data. The measurement data include ice thickness, extent, bulk ice salinity and ice $\delta^{18}O$, as well as seawater salinity, temperature, and $\delta^{18}O$. Additionally, ice crystal and pore structure are examined in relation to these properties.

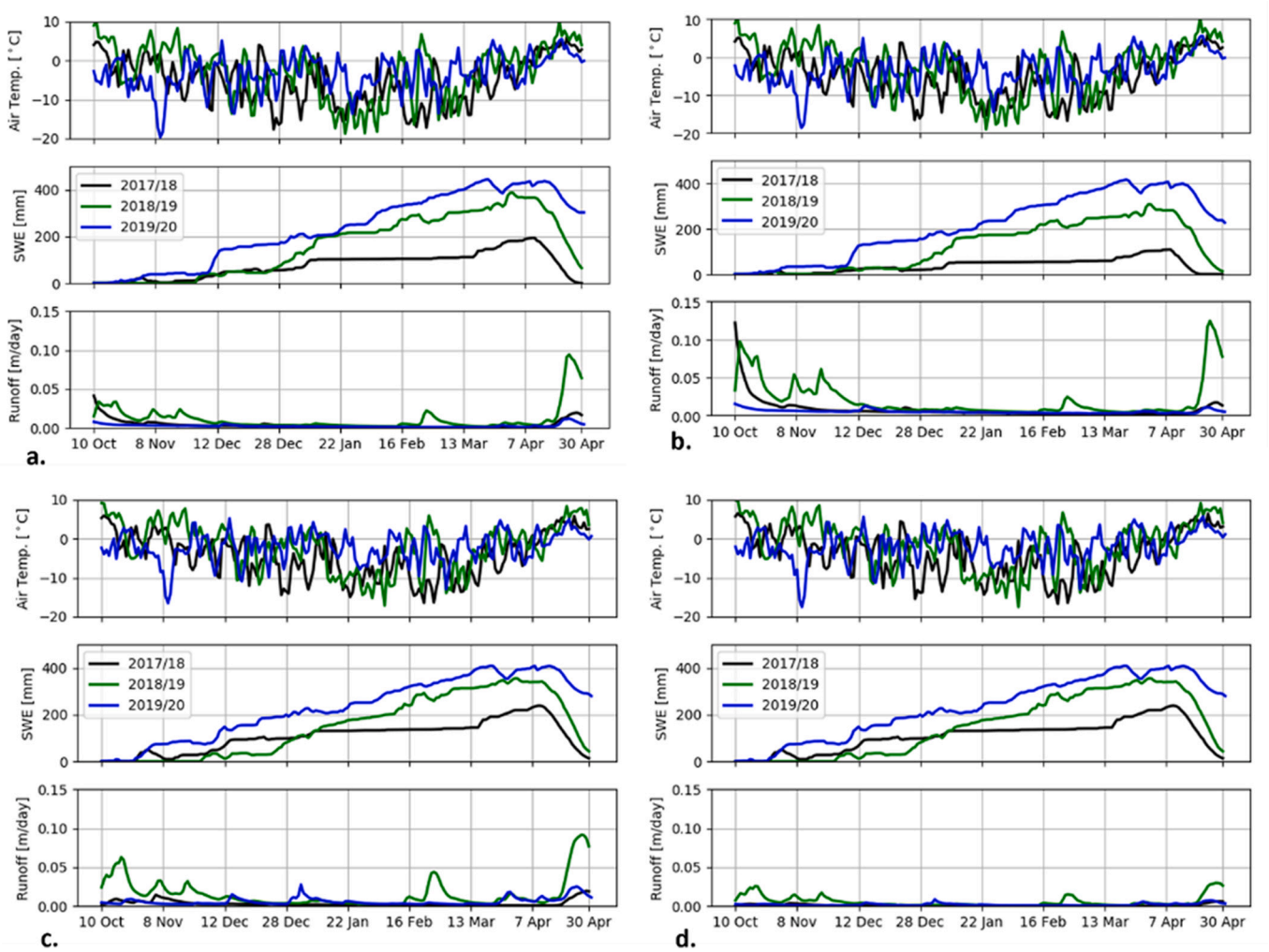

Fig. 9. Spatially interpolated daily average air temperature, accumulated snowfall measured as snow water equivalent (SWE) and runoff ($Q_{fjord,norm}$) for each fjord and year, extracted from seNorge. a) Nordkjosbotn, b) Storfjord, c) Gratangsbotn, and d) Lavangen. Spatially interpolated daily average air temperature, accumulated snowfall measured as snow water equivalent (SWE) and runoff ($Q_{fjord,norm}$) for each fjord and year. e) Beisfjord, f) Ramfjord, g) Kattfjord.

2. Methods

2.1. Study area

Seven fjords located in northern Norway were chosen for ice characterization based on knowledge that they held ice in recent years, determined through satellite imagery and in-situ observation, as well as their accessibility (Fig. 1). Measurements were performed over the winter of 2017/2018, 2018/2019, and 2019/2020 with samples collected toward the end of the ice-growth period (Table 1). In one fjord, Beisfjord, during the 2018/2019 season a transect to collect several cores at increasing distance from the river was also completed.

The fjord Kattfjord (Figs. 1g and 8), is located the furthest north out of the fjords selected. The area of the inner part of the fjord, also referred to as Nordfjorden (Fig. 8), is 5 km long and 1.3 km wide, with a maximum depth of 90 m. Kattfjord has a sharp bend to the northwest accompanied by a decrease in depth to a sill with water depth 54 m and 11 m on each side of an island. Past this point (not shown), the fjord continues before branching in two and eventually meeting the Norwegian sea. The only other fjord that is directly connected to the Norwegian sea, i.e., not being a branch of a larger fjord, is Storfjord (Figs. 1b and 3) which is the inner part of Lyngenfjorden. Being over 80 km long, its head is located further south than Kattfjord while the mouth is further north and leads into the Norwegian sea. Fjord ice formed from the head of the fjord outward 2–3 km, where depth is approximately 33 m and width approximately 1.8 km. Storfjord is primarily straight with no abrupt bends. The nearest sill to the ice edge is roughly 29 m deep and located 8 km from the head of the fjord.

There were two study sites in Balsfjorden; Ramfjord (Figs. 1f and 7) and Nordkjosbotn (Figs. 1a and 2). Ramfjorden stands out amongst the other fjords given the abrupt 90° turn it takes as one first moves northeast into the fjord from Balsfjorden eventually turning to the southeast. From the head of the fjord, depth increases quickly to 56 m before decreasing to the first sill of 22 m depth. As the fjord changes direction, depth again increases to 133 m decreasing only to 118 m at the mouth of the fjord. The width of the fjord is fairly consistent along its 13 km length, being generally 0.7–1 km. Nordkjosbotn (Fig. 2) is a small area located over the innermost 7 km of Balsfjorden. Samples were collected on the eastside of a constriction, <500 m in width, where water depth is only 11 m. To the west of the constriction, depth increases gradually toward the main fjord basin of Balsfjorden.

The remaining three fjords are located over 85 km to the southwest. Both Lavangen (Fig. 1d) and Gratangsbotn (Fig. 1c) are branches of Astafjorden. While near to each other, they differ significantly in depth and geometry. Lavangen (Fig. 5) varies between 1.5 and 2 km in width as it bends smoothly from the southeast to east back to the southeast.

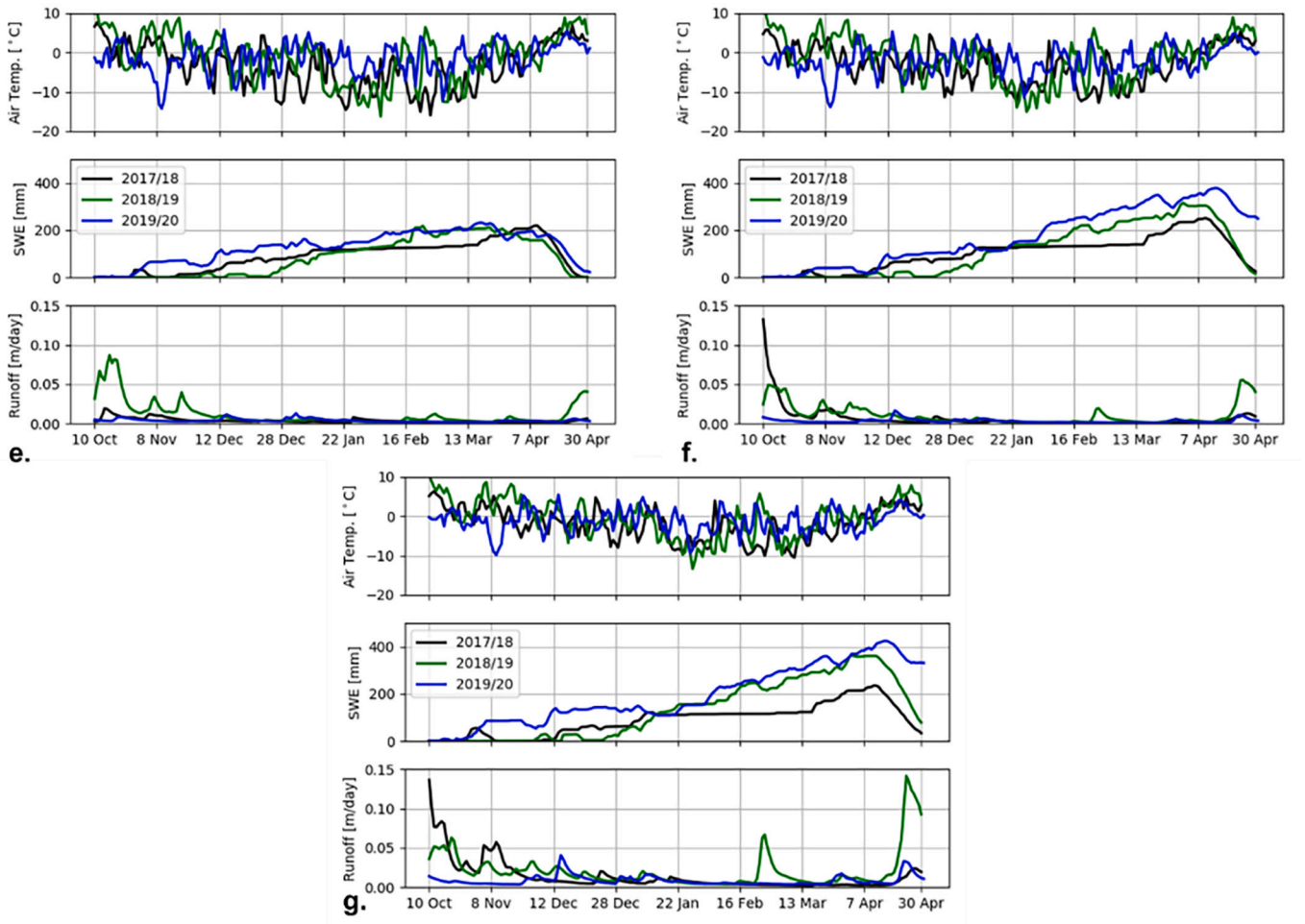

Fig. 9. (*continued*).

Table 2
Freezing degree days in °C days for each fjord and winter season using 0 °C and − 2 °C, calculated for the period 1 Oct-1 May.

	Nordkjosbotn		Storfjord		Gratangsbotn		Lavangen		Beisfjord		Ramfjord		Kattfjord	
	0 °C	−2 °C	0 °C	−2 °C	0 °C	−2 °C	0 °C	−2 °C	0 °C	−2 °C	0 °C	−2 °C	0 °C	−2 °C
2017/18	1159	1136	1134	1115	1008	972	977	943	855	851	777	749	573	537
2018/19	866	846	854	835	702	679	679	651	610	587	592	564	437	401
2019/20	762	732	756	725	560	518	533	495	446	409	516	484	368	313

Measurements were only collected at the head of Lavangen where width decreases to <1 km and depth to <45 m. At its deepest Lavangen measures 202 m with a sill located where it meets Astafjorden about 17 km from the head of the fjord, 106 m deep. In Gratangsbotn (Fig. 4) ice was found to the east of a narrow constriction and sill, 300 m wide and 7 m deep respectively. Depth in the inner part of this part of the fjord, 6 km in length, reaches a maximum of 80–85 m while width is consistently between 0.9 and 1 km. To the west of this constriction, the fjord bends several times over 14 km while depth increases to nearly 200 m before meeting another sill only 30 m in depth.

The furthest south fjord, Beisfjord (Figs. 1e and 6) is a small side fjord to Ofotfjorden. Being 8 km in length, and 0.8–1.0 km wide, depth reaches a maximum of 44 m before a sill with a depth of 23 m. Moving northwest to the head of the fjord, depth stays fairly constant at approximately 24 m before decreasing again to only 3–4 m at the mouth of the fjord. At this point the fjord also narrows from just over 1 km to 350 m.

2.2. Field measurements

Measurements of ice and water were made once a year at each fjord after a solid layer of ice had formed, if any at all. Before ice samples were gathered, any snow on the surface was removed to provide a clean area from which to drill ice cores. At least two cores were taken at each location for ice bulk salinity, stable isotopes, and ice stratigraphy. For salinity measurements, the core was removed and laid horizontal immediately to minimize brine drainage. Using a saw, the core was sliced into 0.05 m sections and double bagged. Samples were melted at room temperature before salinity was measured using a YSI Pro30 temperature/conductivity probe with accuracy of 0.1 on the practical salinity scale (psu) (Fofonoff and Millard, 1983) and resolution of ±0.1 (psu) or ± 1% of the reading, whichever is greater. It is noted that the sampling procedure is meant to minimize brine drainage, but it still can occur being largely dependent on the brine volume fraction (porosity) of the ice. The remaining seawater from the melted ice samples was placed in glass bottles with cone liners and stored at 4 °C for stable oxygen

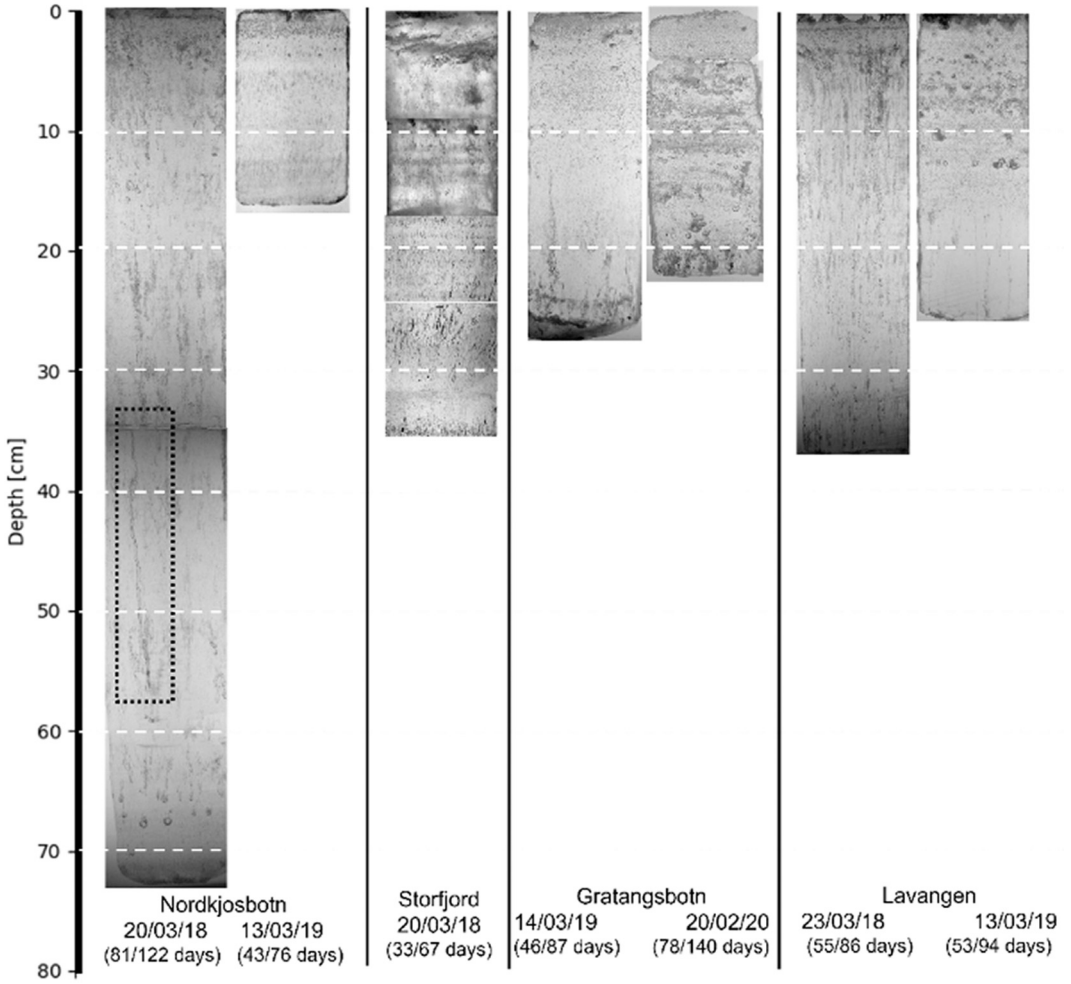

Fig. 10. Backlit vertical thick sections of ice cores to highlight variations in pore structure and density between fjords and years. In general, the less transmittance of light, the greater the scattering of light, signifying a greater number and/or size of pores. To highlight variations in pore shape, the core from Ramfjord is featured in Fig. 18. Dashed boxes used to highlight two elongated pores referenced in text.

isotope analysis. Samples were analyzed at the Stable Isotope Laboratory at the Centre for Arctic Gas Hydrate, Environment and Climate (CAGE) located at UiT The Arctic University of Norway, Tromsø, Norway. A 0.5 mL sample from each melted core slice was pipetted into a 12 mL Labco glass vial which was next flushed with a 0.3% CO2 in He gas mixture, equilibrated at 25 °C for >24 h. Calibration was done through measuring three inhouse standards of $\delta^{18}O$ between −1 and − 36 ‰ that had previously been calibrated against international standards VSMOW2, GISP, and SLAP2. When a line was fit to true vs. measured vales of $\delta^{18}O$, the R^2 value of the line was 1.0, with error between separate readings most often being <0.01‰ but with a standard deviation <0.05‰. A Thermo-Fisher MAT253 IRMS with a Gasbench II was used to measure of the quantity of $\delta^{18}O$.

The stratigraphy core was stored at −18 °C to ensure minimal brine drainage before being sliced in a cold room set to −12 °C. Vertical sections of the stratigraphy core had a thickness of 1–1.2 cm. Using both light transmission and cross-polarizers, ice type and transitions with depth were examined.

For all fjords, seawater temperature and salinity were measured with a CTD (CastAway-CTD, Sontek) at the ice-sampling location just after the ice cores were collected. Slush was removed from one of the holes before measuring the vertical distribution of temperature and salinity in the water column below the ice by lowering the CTD manually from the drill hole to the seabed. The CTD had a resolution and accuracy of 0.01 °C and 0.05 °C respectively for temperature, 0.01 (psu) and ± 0.1 (psu) for salinity, and 0.01 m and ± 0.25% of the measured value for depth. Two casts were made at each location to ensure that consistent measurements were obtained. The data presented here were taken during the upcast, with measurements of pressure, temperature, and conductivity converted to depth and salinity automatically by the instrument using the UNESCO equations (Fofonoff and Millard, 1983). The CTD sampled at a frequency of 5 Hz and was raised at approximately 0.5 m/s. Only upcasts were used due to the presence of ice that sometimes formed around the sensor while in between measurements. This resulted in a clear error in measurements of the upper water column in the downcast as the ice was melted and/or dislodged. Seawater samples from 0.20 down to 2.0 m below the bottom of the ice were collected for isotopic measurements using a manual water pump attached to a rubber hose. The hose was rinsed with water from the desired depth and two cone-lined bottles were filled and stored at the lab facility at SINTEF Narvik at 4 °C until analysis at the UiT stable isotope laboratory.

2.3. External measurements

2.3.1. Determining ice freeze up and break up

UOVision UM 565 and UM785 trail cameras were used to collect time-lapse images at all fjords except Nordkjosbotn. This allowed for tracking of weather events as well as determination of ice freeze up and

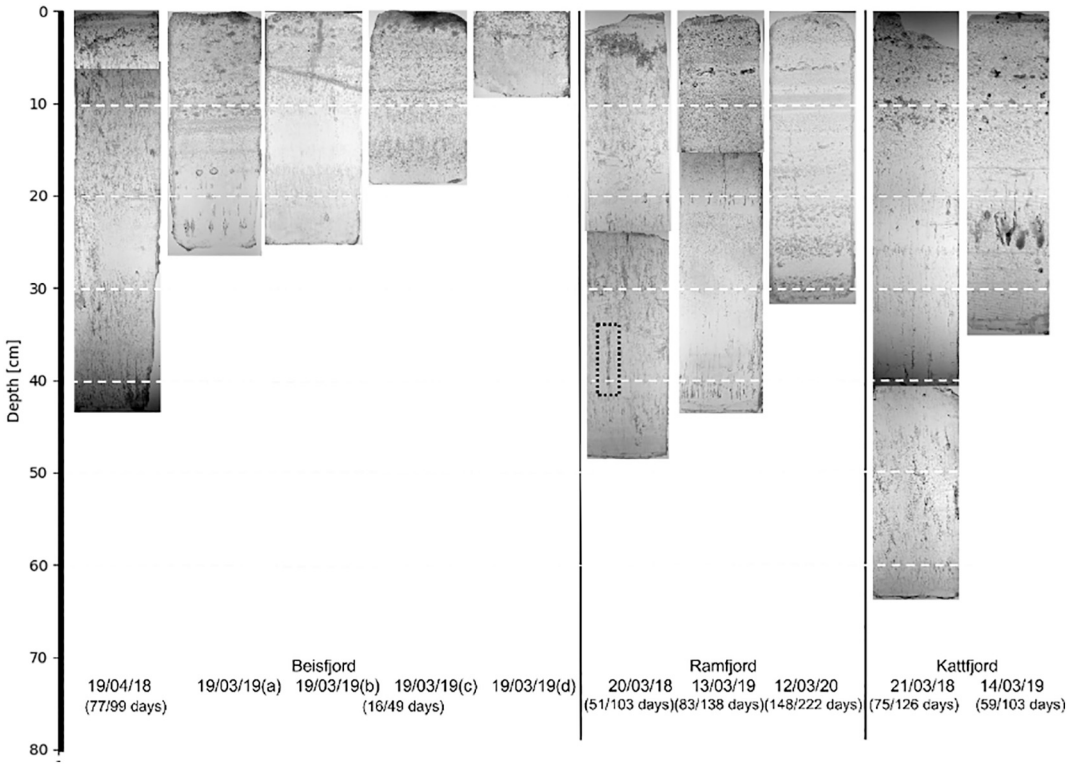

Fig. 10. (*continued*).

break up. As images were only gathered in the last season, 2019–2020, satellite imagery was needed to track the formation and breakup of ice during the first two seasons. Two products were used for this purpose - SENTINEL-1C-band Synthetic aperture radar (SAR) and imagery from Terra satellite MODIS sensor, specifically the MOD09A1.006 Terra Surface Reflectance 8-Day Global 500 m product (Copernicus Sentinel data 2019). For the former, Ground Range Detected (GRD) scenes were evaluated with Google Earth Engine (Gorelick et al., 2017). Processing steps for MODIS imagery were described in detail by O'Sadnick et al. (2020). Ice formation and break up can occur several times throughout the season. Here, freeze up is defined as the first day of consistent ice coverage, with no further break ups occurring before the day of measurement. The ice edge often deteriorated over time, with rarely a single event leading to all ice dispersing. The date of break up provided here represents the first day where the fjord was entirely ice free.

2.3.2. Weather data and calculation of freezing degree days

Values for average daily air temperature, accumulated snow cover, and runoff were obtained from the openly available web portal seNorge.no (Lussana et al., 2018), providing spatially interpolated observational data by the Norwegian Meteorological Institute and the Norwegian Water Resources and Energy Directorate (NVE). Values for both runoff and accumulated snow cover are derived using the Hydrologiska Byråns Vattenbalansavdelning (HBV) hydrology model. Runoff (Q) in m/day is a function of several parameters including precipitation and evapotranspiration as well as changes over time in the amount of water stored in the soil, snow, and bodies of water (Bergström, 1992).The resolution of the HBV model is 1 km. The following approach was used to find the normalized daily runoff ($Q_{fjord,\ norm}$) for each fjord:

$$Q_{\mathrm{fjord},norm} = \frac{Q_{\mathrm{fjord}}}{A_{\mathrm{fjord}}} \tag{2}$$

$$Q_{\mathrm{fjord}} = \sum_{WS\ 1} Q_{pixel} + \sum_{WS\ 2} Q_{pixel} + \ldots \tag{3}$$

$$Q_{pixel} = QA_{pixel}F \tag{4}$$

where A_{pixel} is the area of a pixel equal to approximately 10^6 m^2, F = fraction of the pixel within the watershed (WS), Q_{pixel} is the volume of runoff for a pixel in m^3/day, Q_{fjord} is total volume of runoff leading into the fjord in m^3/day based on each individual watershed (WS), and $Q_{fjord,\ norm}$ is the amount of runoff into the fjord normalized by A_{fjord}, given in m/day (m^3/day per m^2). Boundaries of water sheds were provided by NVE through their watershed database, REGINE (Nedbørfelt (REGINE), 2020). Fjord area is defined here as the area of the fjord connected to these watersheds. In Figs. 2- 8, the area of the fjord shown is approximately the area of the fjord used in these calculations.

Accumulated snow cover and air temperature presented here come from the selection of one pixel at the head of each fjord, located at sea level. While this method does not account for variability throughout the fjord it provides a general view of temperature and snow conditions at sea level.

To better understand the overall potential for ice growth in each fjord, freezing degree days (FDDs) were calculated from 1 October to 1 May. Additionally, FDDs were calculated starting from the day of ice formation in each individual fjord until the day ice thickness was measured. FDDs are derived by summing all average daily air temperatures (T_a) below freezing point (T_f) from a start date ($i = 1$) to end date ($i = \mathrm{N}$):

$$FDD = \sum_{i=1}^{N} \Delta t \begin{cases} T_f - T_{a,i}, & T_{a,i} < T_f \\ 0, & T_{a,i} \geq T_f \end{cases} \tag{3}$$

Here $\Delta t = 1$ day. Given the uncertainty in the salinity of the surface water at the time of ice formation, FDDs were calculated for both T_f = 0 °C, representing freezing temperature of fresh water, and $T_f = -2$ °C representing sea water. Freezing degree days are useful in the prediction of ice thickness which is approximated in the following using the equation derived by (Anderson, 1961),

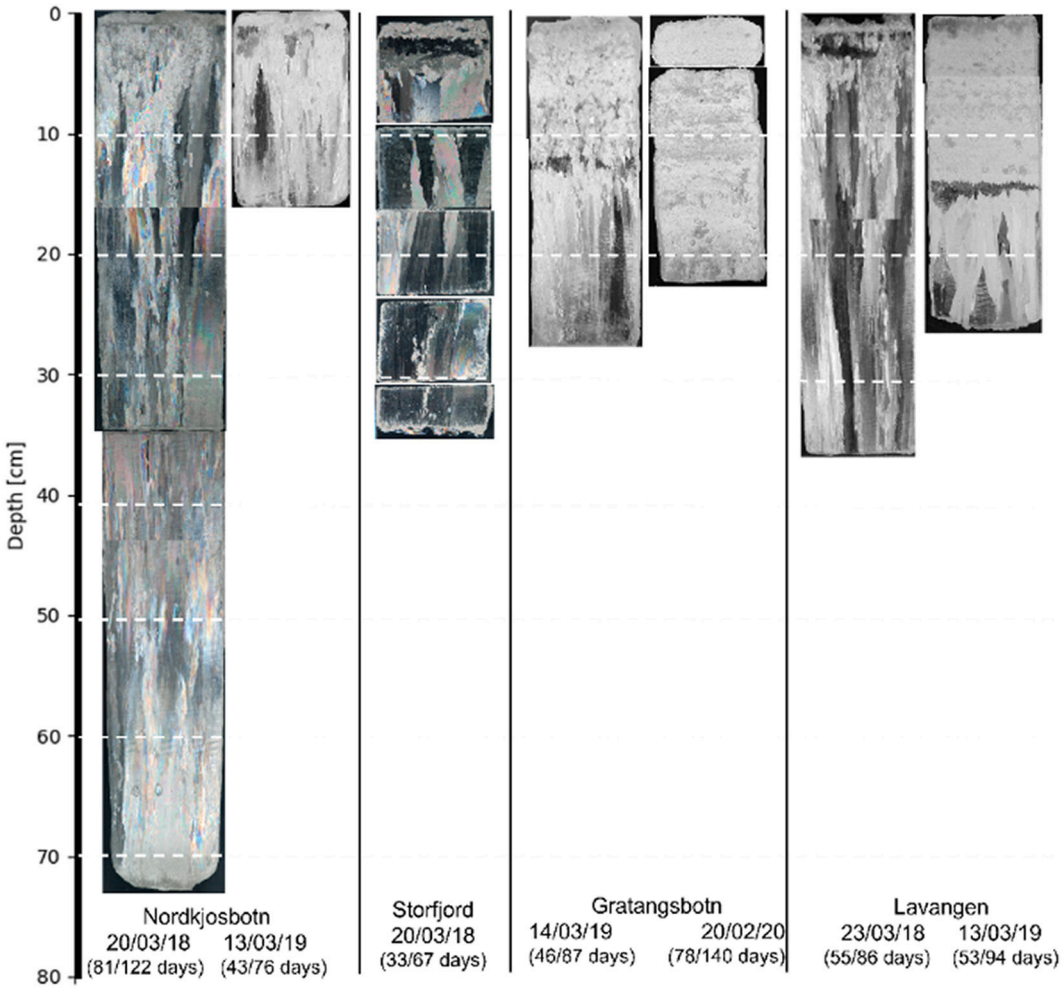

Fig. 11. The same vertical thick sections as shown in Fig. 9, seen through cross-polarized filters to highlight transitions in ice crystal structure. Smaller crystals, less homogeneous in shape, size and orientation are characteristic of granular ice, typically located in the upper part of the core. Elongated crystals are identified as columnar ice.

$$H^2 + 5.1H = 6.7\theta \quad (4)$$

where H is ice thickness in cm and θ is freezing degree days in °C days. In this work, fjords are primarily ordered according to freezing degree days, moving from the fjord with the highest value of FDD (coldest) to the lowest (warmest).

3. Results

3.1. Weather conditions

Storfjord and Nordkjosbotn where the fjords with lowest air temperatures, as displayed by the number of FDDs each year with temperatures frequently dipping below −10 °C or as in the 2017/18 season, below −15 °C (Fig. 9, Table 2). Kattfjord had the highest air temperatures consistently above −10 °C throughout the winter (Fig. 9b) and the lowest numbers of FDDs.

For all fjords but Beisfjord, the lowest values of accumulated snowfall on land adjacent to the fjord occurred during the 2017/18 season and the highest values during the 2019/20 season. In Beisfjord, 2019/2020 began with higher values of snowfall but did not maintain the consistent increase shown in other fjords. Additionally, Beisfjord had the lowest snowfall values in comparison to other fjords for the last two seasons.

For all fjords, runoff was generally low between December into March and even April except in Kattfjord where events leading to runoff (i.e., warm spells) occurred all three years in January. Another exception can be seen at the end of February during the 2018/19 season, when the runoff increased in all fjords, being largest in Kattfjord and smallest in Beisfjord.

3.2. Length of time with ice cover, ice thickness, and ice area

The observed duration of ice cover and thickness of ice varied between fjords and between years (Table 1). The longest period of consistent ice coverage, 222 days, occurred in Ramfjord during the 2019/20 season. For Kattfjord, Storfjord, Gratangsbotn, and Beisfjord, 2017/18 had the longest period of ice coverage while Lavangen had a nearly the same length of time with ice in the first two seasons, with a shorter season during 2019/2020. Ice was thickest for all fjords on the day of measurement in 2018 except for Gratangsbotn where no consistent ice cover was observed. In contrast, ice extent on the day of measurement was greatest in 2019 for all except Storfjord and Beisfjord with both having the greatest extent of ice in 2018 (Figs. 2 – 8).

3.3. Ice core measurements

The ice core measurements revealed large variability in ice structure

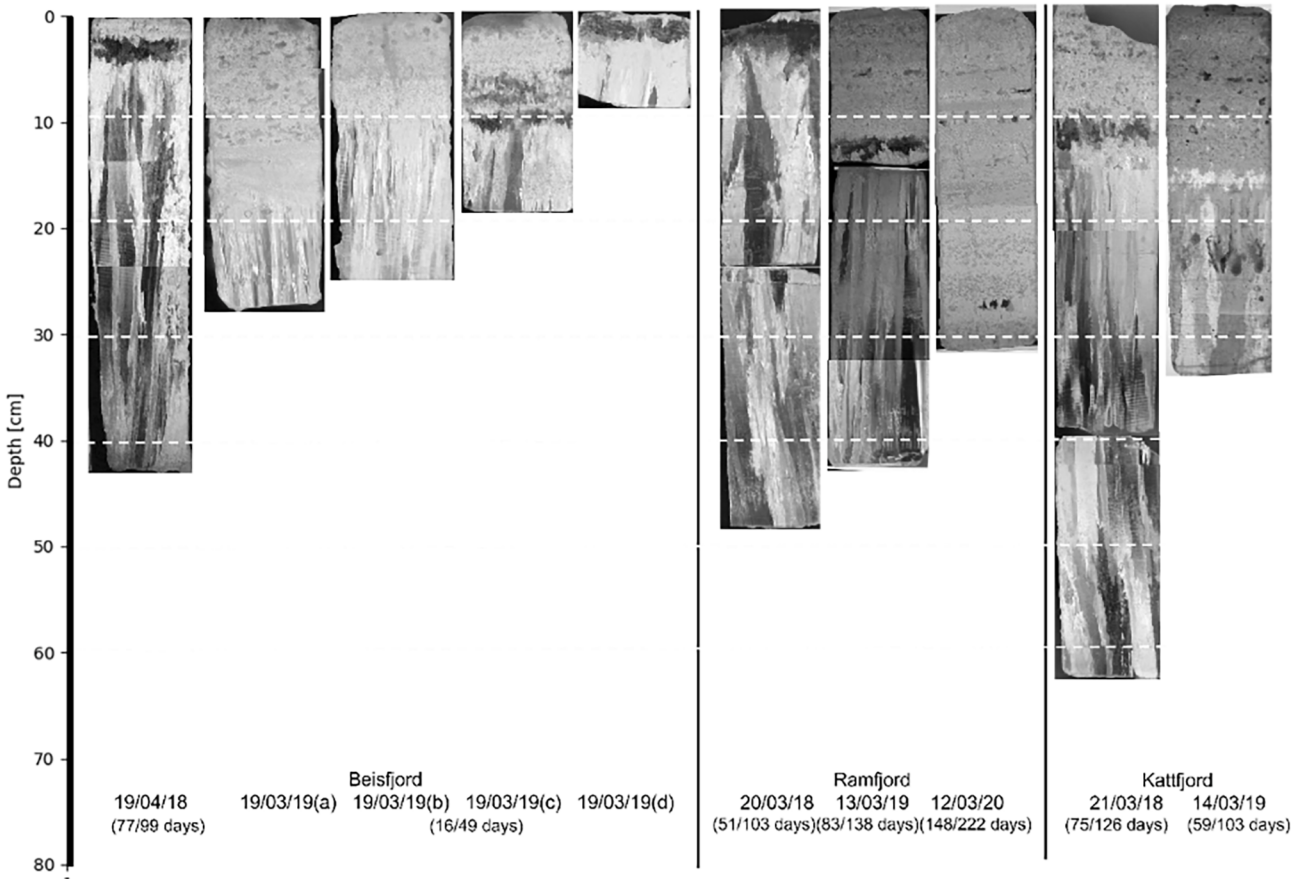

Fig. 11. (*continued*).

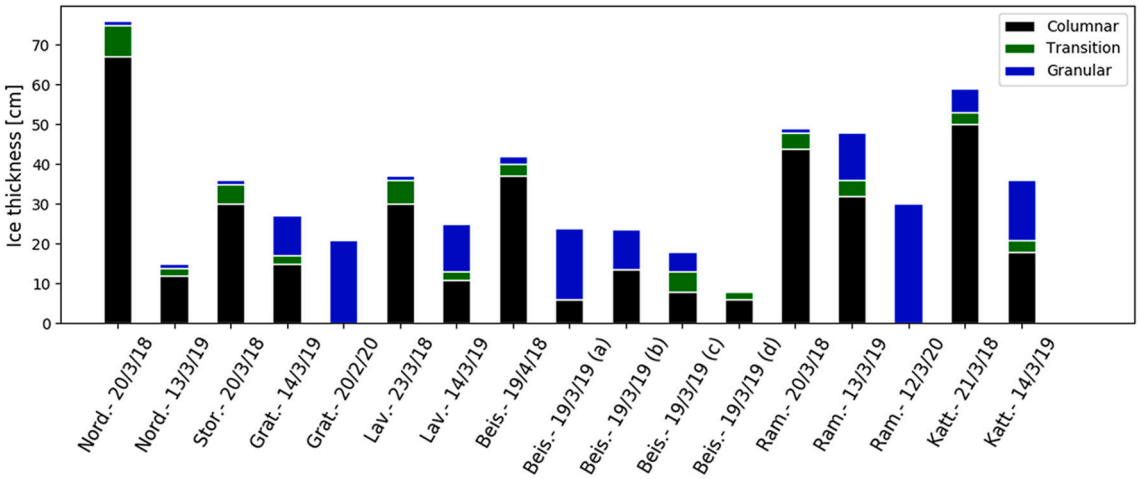

Fig. 12. Simplified view of cores showing division between columnar, transition, and granular ice. For further information on cores, see Table 1.

and crystallography between fjords and years (Figs. 10 and 11). The greatest fraction of congelation ice was found in 2018 (Fig. 12). The following year, cores had a mixture of columnar and granular ice while in the final year, the two fjords where ice was sampled had cores composed entirely of granular ice (Fig. 12). When the ice cores were illuminated only by light (Fig. 10), layers of pores differing in size and shape, changing between years and fjords, are apparent within both granular and congelation ice. In the latter, cores from 2018 season have the most examples of elongated pores, characteristic of saline sea ice, for example in Nordkjosbotn where a brine pore runs from 35 to 55 cm depth. In Ramfjord, a pore approximately 6 cm in length is also visible (marked in Fig. 10). However, in all other cores, pores are generally thinner (approximately <1 mm) and shorter (approximately <2 cm) or inhomogeneous in shape with layers of spherical or asymmetric pores varying in density.

3.4. *Ice core measurements – salinity and $\delta^{18}O$*

Profiles of ice bulk salinity and $\delta^{18}O$ are shown in Fig. 13. The fjord with the highest bulk salinity and $\delta^{18}O$ throughout the entire core came

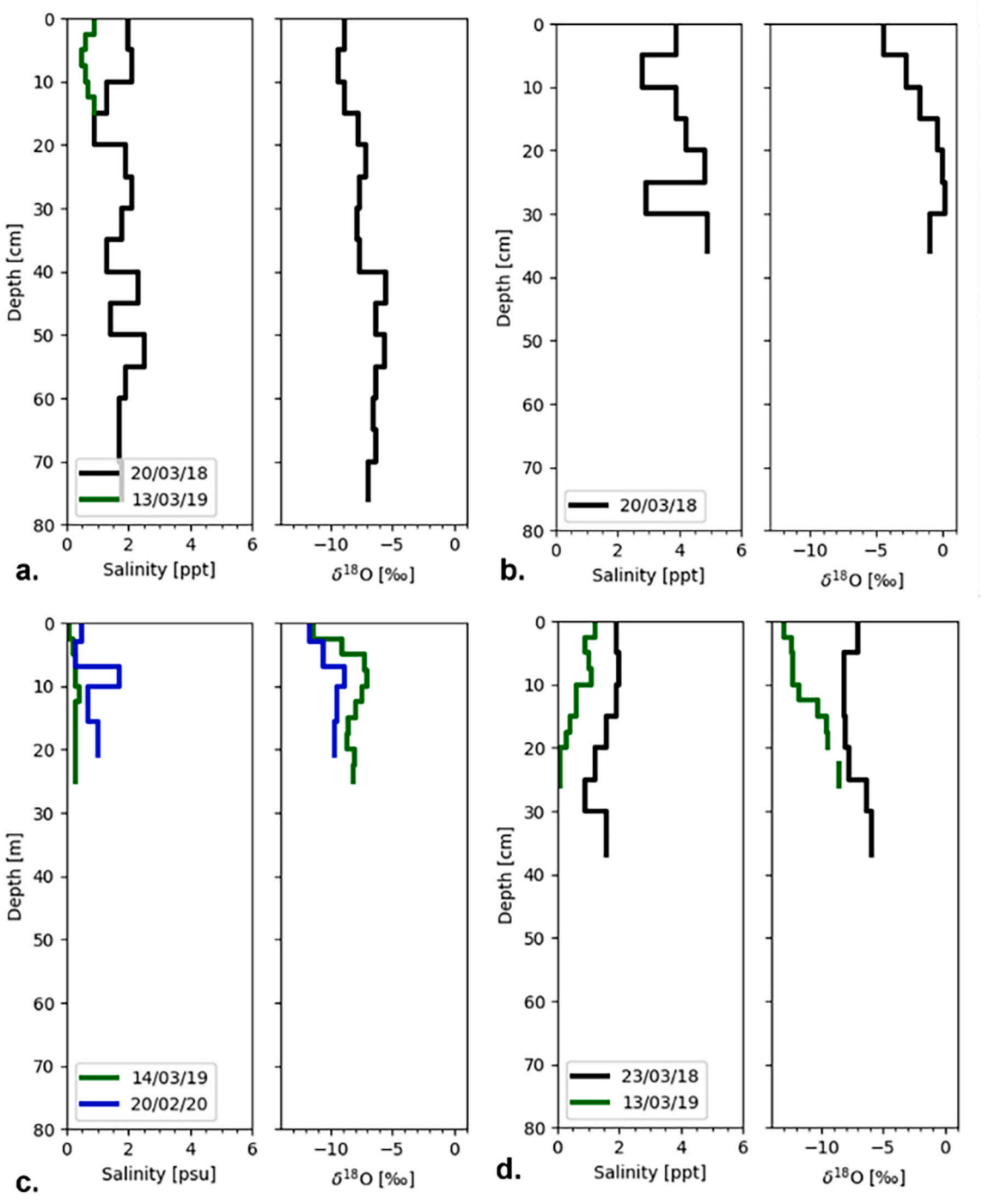

Fig. 13. Profiles of bulk ice salinity and $\delta^{18}O$ for a) Nordkjosbotn, b) Storfjord, c) Gratangsbotn, and d) Lavangen. Profiles of bulk ice salinity and $\delta^{18}O$ for e) Beisfjord, f) Ramfjord, and g) Kattfjord.

from Storfjord in March 2018. Second to this is a core gathered in Beisfjord in 2019/20 that had high values of salinity in the upper 10 cm granular ice that quickly decreased as depth increased. In all other cores, bulk salinity did not exceed 3 psu with measurements being as low as 0 psu.

3.5. Seawater – CTD measurements

CTD measurements reveal a relatively large variation in water temperature between the three field campaigns (Fig. 14). The coldest water for all seven fjords was measured in March 2018. In all three years the four furthest north fjords (Nordkjosbotn (Fig. 14a), Storfjord (Fig. 14b), Ramfjord (Fig. 14f), and Kattfjord (Fig. 14g)) were cooler than the southern three (Gratangsbotn (Fig. 14c), Lavangen (Fig. 14d), and Beisfjord (Fig. 14e)), most noticeably in 2018 with the latter three fjords being upwards of 2 °C warmer. All fjords had water temperature above 0 °C except Storfjord where a temperature of −0.11 °C was measured in March 2018, which was the only year with measurements and ice in this location.

At depths >1 m below the ice-ocean interface, salinity remained

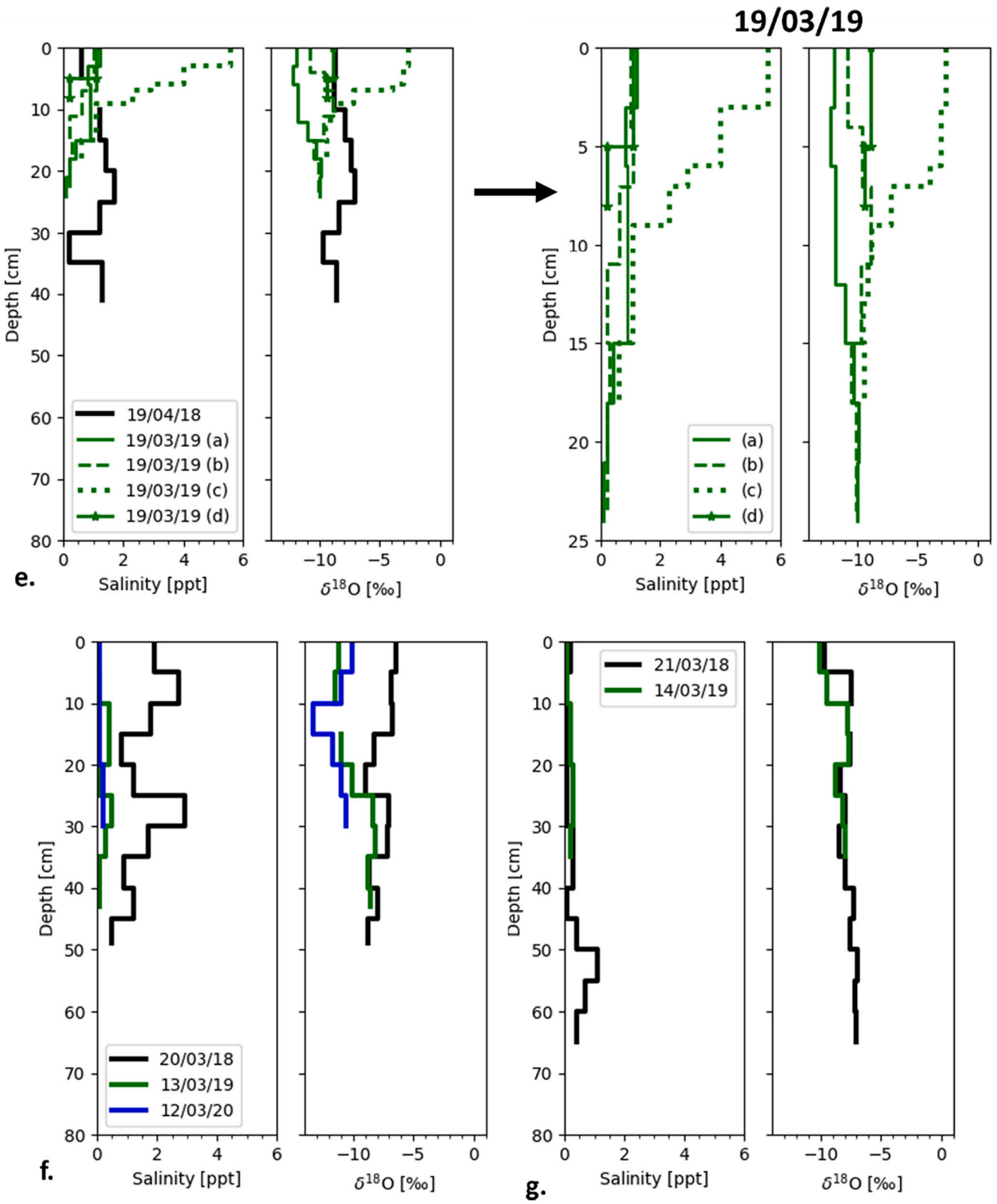

Fig. 13. (*continued*).

consistently above 32 psu for four fjords – Gratangsbotn, Nordkjosbotn, Storfjord, and Ramfjord. In Beisfjord, ocean salinity was slightly lower than the other fjords at depth being between 31 and 32 psu all three seasons. When density is considered, all fjords display an increase with depth with values ranging consistently between 1025 and 1027 kg/m^3 except for the uppermost measurements in Gratangsbotn, Lavangen, Beisfjord, and Ramfjord that dropped to, at a minimum, 1020 kg/m^3. From these CTD measurements, it is apparent that all fjords were stably stratified.

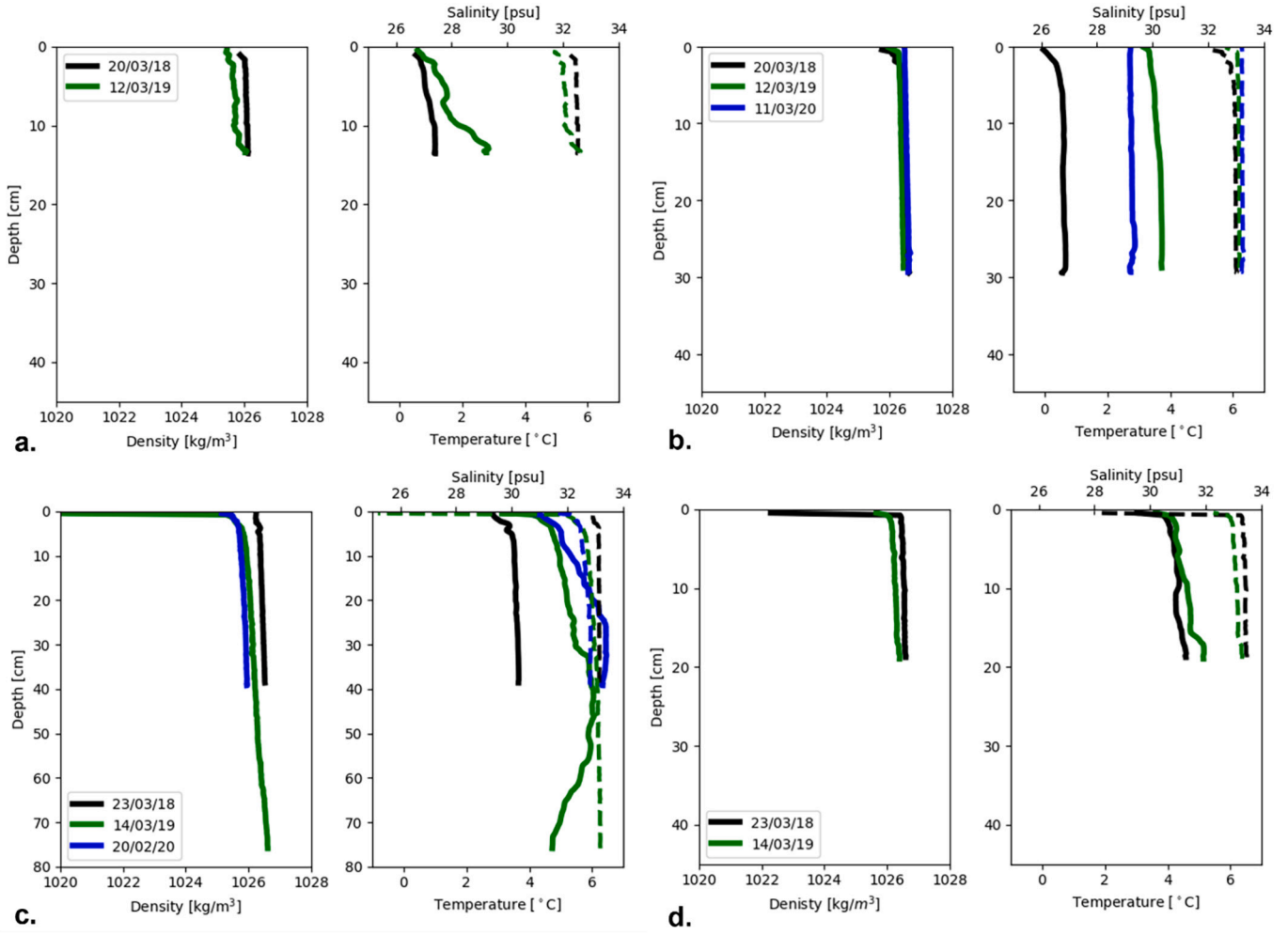

Fig. 14. Profiles of seawater salinity (dashed line) and temperature (solid line) for each fjord and year. Zero depth represents the ocean surface with measurements starting at or slightly below the ice-ocean interface. a) Nordkjosbotn, b) Storfjord, c) Gratangsbotn, and d) Lavangen. Profiles of seawater salinity (dashed line) and temperature (solid line) for each fjord and year. Zero depth represents the ocean surface with measurements starting at or slightly below the ice-ocean interface. e) Beisfjord, f) Ramfjord, and g) Kattfjord.

3.6. $\delta^{18}O$ in river, ocean and snow

The lowest $\delta^{18}O$ value measured of −13.02 ‰ occurred in the snow of Ramfjord in 2019 (Table 3). River values of $\delta^{18}O$ were near to that of snow but show differences between fjords. In Ramfjord and Nordkjosbotn, river water consistently had values of $\delta^{18}O$ below −12 ‰. For Storfjord, Ramfjord and Lavangen, $\delta^{18}O$ ranged between −11 and − 12 ‰ while Kattfjord was consistently between −10 and − 11 ‰. Gratangsbotn had a higher value of −10.86 ‰ in 2019 in comparison to 2020 where $\delta^{18}O$ was measured to be −11.25 ‰. Ocean water gathered at depths ranging from 0.8 m to 1.5 m from the bottom of the ice, had $\delta^{18}O$ values ranging between −1 and 0 ‰ with only two instances of lower values in 2019, in Ramfjord and in one location in Beisfjord.

4. Discussion

Clear variations were observed in ice thickness, crystal structure, and properties between fjords and years. Here the drivers of ice formation and the differences in ice properties between seasons and fjords are examined. Analysis and discussion are included of the relationship of ice thickness and pore structure to several weather-related variables to better understand if and to what extent each may influence ice formation in a fjord environment. In addition, the relation to fjord geometry and bathymetry with focus placed largely on the influence of freshwater flow into the fjord and the creation and persistence of a brackish surface layer is presented.

4.1. Freezing degree days and the prediction of ice thickness

With lower temperatures and a greater number of freezing degree days comes thicker ice as defined by Eqns. 3 and 4 above. However, in the data presented here, this relationship is at times weak and inconsistent. While there is a significant positive correlation ($p = 0.012$) between ice thickness and freezing degree days accumulated from the start of ice formation until the date of the thickness measurement during the 2017/18 season (Fig. 15), ice growth in the 2018/19 season appears to be almost independent of this value. During the latter season, observed ice thickness ranged from 0.15 to 50 cm although FDDs only varied slightly, falling around approximately 350 °C days for all except the Beisfjord core. The number of measurements in season 2019/20 was too low to draw conclusions. Eqns. 3 and 4 provide a starting point to examine the connection between air temperature, ice growth and the factors that may disrupt this relationship. Surface melt, for example, is not included in this estimation although it can contribute to ice thickness being less than that predicted (Fig. 15). The longest period of above freezing average daily air temperatures experienced by all fjords

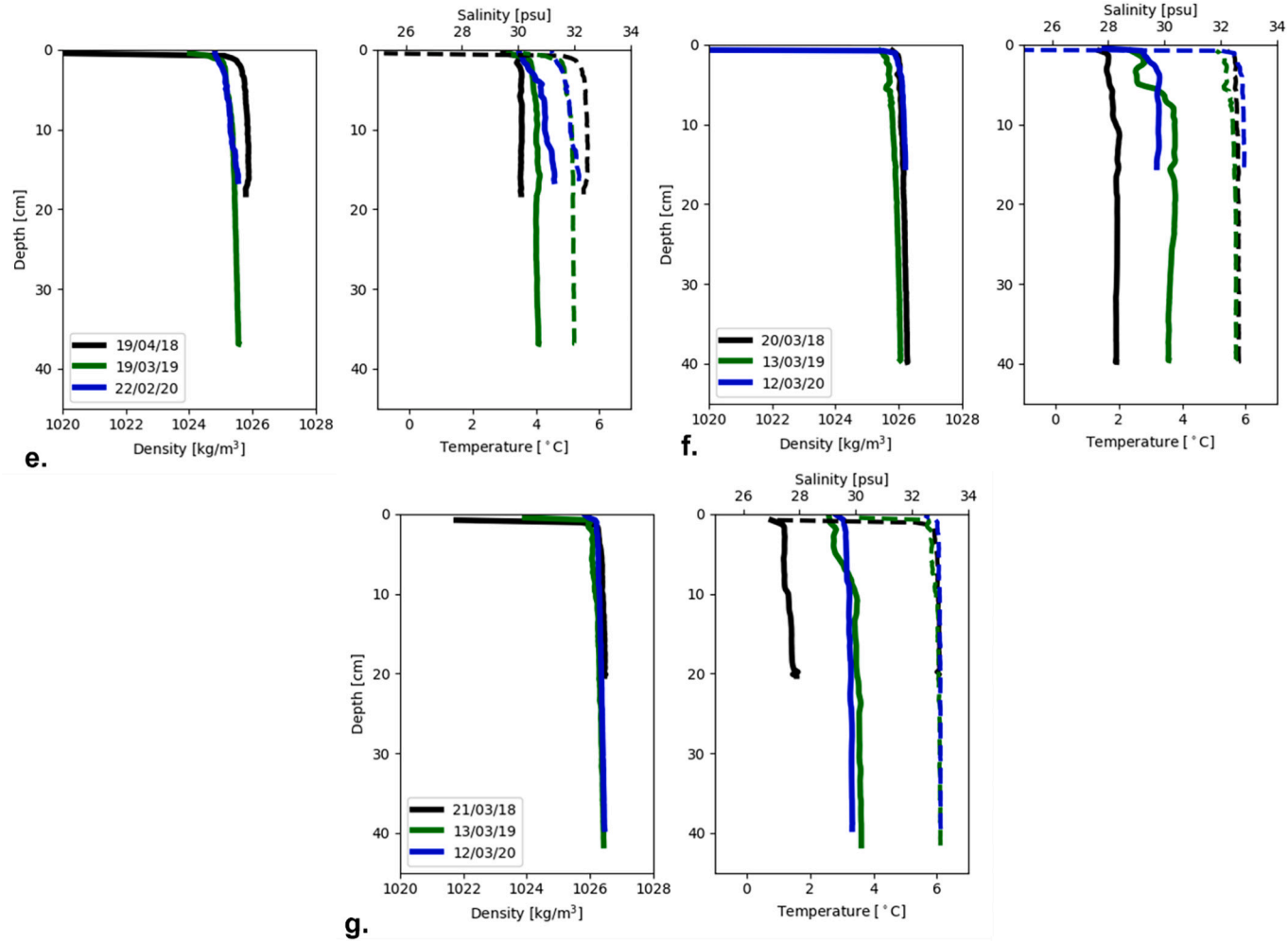

Fig. 14. (*continued*).

occurred from approximately 23–28 February 2019. Outside of this event, such periods of above freezing temperatures generally lasted only 1–3 days. The only exception was during the notably long 2019/20 season at Ramfjord, where average air temperature was above 0 °C from 7 to 14 January 2020. With above freezing days scattered amongst days of below freezing temperatures, surface melt has potential to refreeze forming superimposed ice further complicating estimations of ice thickness.

Oceanic heat flux is another, likely significant, contributor to the disagreement between calculated and measured ice thickness. Being dependent on coastal and tidal currents, the shape and depth of the fjord, and seasonal evolution of currents and temperature, oceanic heat flux is non-trivial to determine, and requires time series of measurements from a highly variable environment. Future work examining the topic of oceanic heat flux and its relationship to ice in fjords will therefore use detailed measurements of ocean temperature, salinity, and currents in combination with numerical model simulations.

Retardation of ice growth due to the insulating properties of snow and formation of snow-ice are also candidates that could explain the failure of FDDs to explain ice thickness in season 2018/19. To investigate the impact of particularly snow, we compare snow cover, expressed as snow water equivalent (SWE) on the day of measurement, to measurements ice thickness across all three seasons in Fig. 16. The significant relationship ($p = 0.014$) supports that higher cumulative snowfall over the entirety of the season, 1 October – 30 April, is associated with thinner ice in the cores gathered. While this relationship is not apparent in the winter of 2017/18 we attribute this to a larger snowfall event only several days before field observations therefore having minimal influence on ice growth.

While the retarding effect of snowfall on ice thickness may be intuitive there is another, contradictory, impact of snow at work - its ability to increase ice thickness from the ice surface, upwards. In Ramfjord, as noted above, the composition of the ice between the three years varied substantially, from majority congelation ice, to a mixture between congelation and granular ice, to entirely granular on the day of measurement the last season (Figs. 11 & 12). Therefore, while snow may have slowed ice growth for years where a solid layer of congelation ice was present, snow also likely played an important role in thickening ice at times, for example in 2019/20. The identification of snow ice in comparison to columnar ice using $\delta^{18}O$ is a common method to determine the fraction of each ice type. In the cores studied here, this approach is complicated by the substantial amount of meteoric water, water that originates as precipitation like rain or snow including runoff from rivers, in the upper water column contributing to ice formation. Low values for $\delta^{18}O$ cannot therefore be attributed to only snow ice but also frazil or congelation ice formed from fresh or brackish water or snow flooded by fresh and brackish water instead of seawater. Each will have a distinct signature for $\delta^{18}O$ that reflects both the mixture of fresh and ocean water present at the ice-ocean interface and growth rate. The samples collected show $\delta^{18}O$ values consistently below 0‰, the point often used as the delineator between snow ice and congelation sea ice (Eicken et al., 1994; Jeffries et al., 1994; Smith et al., 2012). The only core with values above 0‰ was taken in Storfjord. Granular ice having a lower $\delta^{18}O$ value is present in the upper 5 cm however as ice transitions

Table 3
Measurements of $\delta^{18}O$ taken from seawater with depth below the ice surface in m marked in parentheses, river leading into the fjord, and snow on top of the ice. n/m = not measured.

Nordkjosbotn				Storfjord			
Date of measurement	$\delta^{18}O$ [‰]			Date of measurement	$\delta^{18}O$ [‰]		
	Seawater	River	Snow		Seawater	River	Snow
20 Mar 2018	n/m	n/m	n/m	20 Mar 2018	−0.17 (1.5)	n/m	n/m
13 Mar 2019	−0.17 (1.5)	−12.15	n/m	12 Mar 2019	−0.08 (1.5)	−11.55	n/m
12 Mar 2020	n/m	−12.30	n/m	11 Mar 2020	0.09 (1.5)	−11.82	n/m

Gratangsbotn				Lavangen			
Date of measurement	$\delta^{18}O$ [‰]			Date of measurement	$\delta^{18}O$ [‰]		
	Seawater	River	Snow		Seawater	River	Snow
23 Mar 2018	−0.28 (0.4)	n/m	n/m	23 Mar 2018	−0.12 (1.0)	n/m	n/m
14 Mar 2019	−0.92 (1.0)	−10.86	−12.55 (at surface)	14 Mar 2019	−0.53 (1.0)	−11.34	n/m
20 Feb 2020	−2.42 (1.0)	−11.25	n/m	2020	n/m	n/m	n/m

Beisfjord				Ramfjord			
Date of measurement	$\delta^{18}O$ [‰]			Date of measurement	$\delta^{18}O$ [‰]		
	Seawater	River	Snow		Seawater	River	Snow
19 Apr 2018	−0.56 (1.0 m)	−12.57	n/m	20 Mar 2018	−0.81 (1.5)	n/m	n/m
19 Mar 2019	−1.57 to - 0.7 (1.4 m)	−12.49	n/m	13 Mar 2019	−1.06 (0.80)	−11.14	−13.02 (surface)
22 Feb 2020	−0.81 (1.5 m)	−12.52	n/m	12 Mar 2020	−0.51 (1.0)	−11.55	nm

Kattfjord			
Date of measurement	$\delta^{18}O$ [‰]		
	Seawater	River	Snow
21 Mar 2018	−0.12 (1.5)	n/m	n/m
14 Mar 2019	−0.72 (0.80)	−10.24	−11.94 (surface)
12 Mar 2020	−0.16 (1.5)	−10.65	n/m

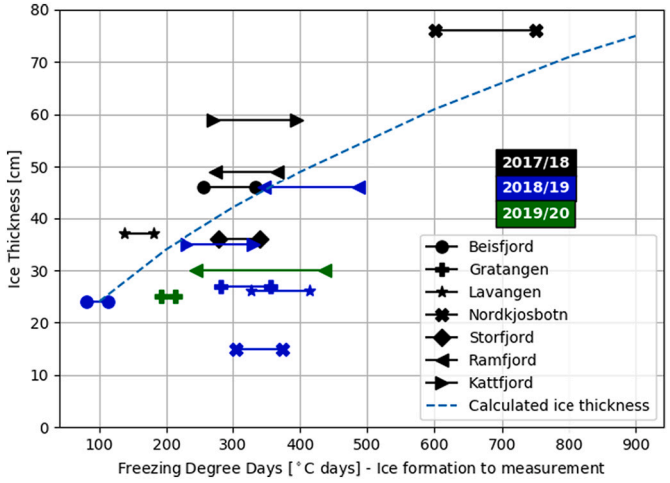

Fig. 15. Ice thickness compared to freezing degree days calculated from the day of ice formation to measurement for 2017/18 season (black), 2018/19 season (blue), and 2019/20 season (green). Two values for each fjord are shown connected- FDDs calculated using −2 °C and 0 °C. The dashed line represents the calculated ice thickness (Eq. 4). (For interpretation of the references to colour in this figure legend, the reader is referred to the web version of this article.)

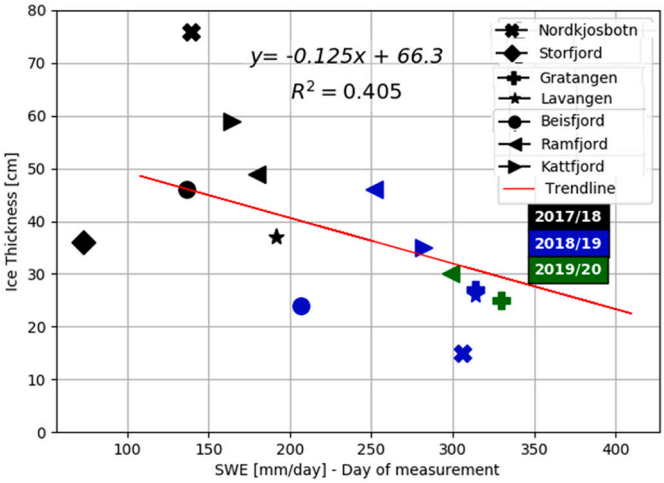

Fig. 16. Ice thickness compared to snow water equivalent (SWE) on the day of measurement for 2017/18 season (black), 2018/19 season (blue), and 2019/20 season (green). The solid line represents the linear trend fitted to the data with equation and R^2 marked also provided. (For interpretation of the references to colour in this figure legend, the reader is referred to the web version of this article.)

to congelation ice, $\delta^{18}O$ is shown to increase gradually with no abrupt jumps to signal a boundary.

The proportion of snow ice is an important factor to consider as it can have an impact on, for example, the biologic productivity of the ice (Granskog et al., 2003), the approach to accidents like an oil spill (Oggier et al., 2019), the interaction between ice and structures (Timco and Weeks, 2010), and how ice conditions may evolve through the

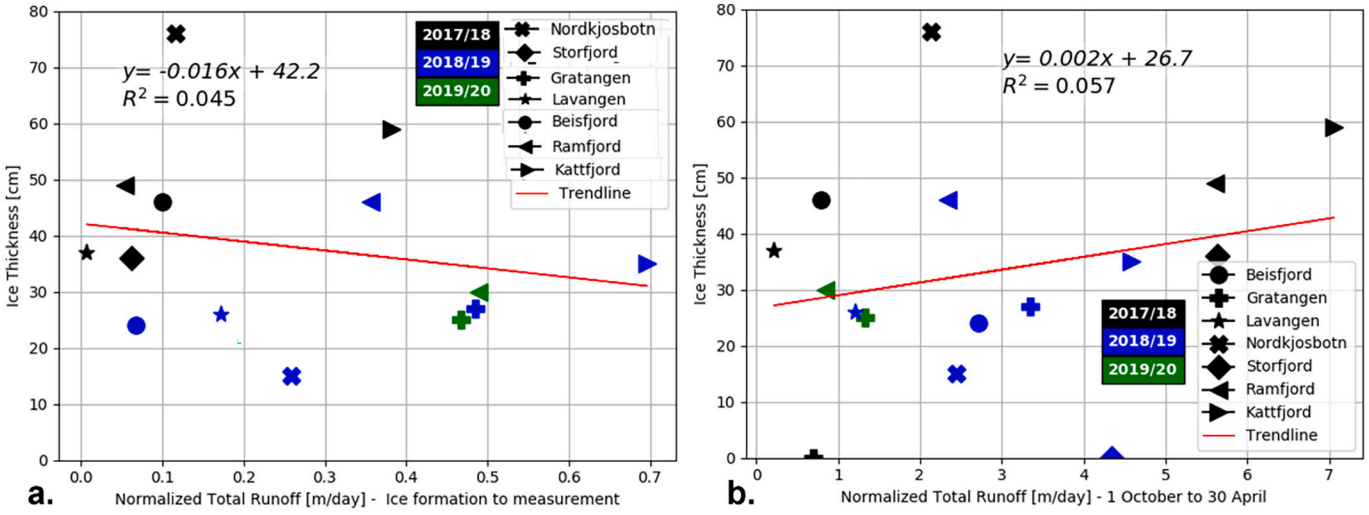

Fig. 17. Ice thickness compared to total runoff up to the day of measurement (a) and over the entire season (b) for 2017/18 season (black), 2018/19 season (blue), 2019/20 season (green). The line represents the linear trend fitted to the data. The trends are not significantly different from 0. (For interpretation of the references to colour in this figure legend, the reader is referred to the web version of this article.)

season (Polashenski et al., 2012). The timing of snowfall events, air and ocean temperature, and other variables like wind and tides that cause mixing, can all contribute to the balance between congelation and granular ice growth- this topic specific to a fjord environment would benefit from further examination.

Another factor that may impact the relationship between freezing degree days and ice thickness and the general formation of ice growth in fjords is freshwater which, when combined with limited mixing with the saline ocean water below, can cause a decoupling between the surface and intermediary layer. Through cooling of this upper-most surface layer, ice can begin to form. For ice grown from seawater of approximately 33 psu, ice bulk salinity values between 4 and 8 psu have been both modelled and observed during the ice growth phase in the Arctic (Petrich and Eicken, 2010; Petrich et al., 2011). Measurements of ice bulk salinity primarily below 3 psu and often below 1 psu, are indicative of brackish or fresh water at the ice-ocean interface at the time of ice growth yet ocean salinity on the day ice cores were gathered was not often measured below 31 psu. For the fjords considered, there was an insignificant relationship found between ice thickness and total runoff from ice formation to the day of measurement and over the entire season ($p = 0.466$ and $p = 0.372$ respectively) (Fig. 17). When a linear relationship is applied, the two show opposing relationships- runoff and ice thickness being negatively correlated when considering only the ice growth period, and positively related when the entire season is considered. In both cases however, the spread of values is large. The brackish or fresh water was, therefore, likely confined to a temporary layer at the ice–ocean interface controlled by the amount of freshwater flow leading into the fjord and mixing by tides and currents.

While the number of variables at play in a fjord environment makes it difficult to determine the influence of freshwater flux on ice growth rate, its most significant role may come during the initial formation of the ice. Fresh water will mix with the upper surface layer of the ocean as it enters the fjord, decreasing its salinity to become brackish and decreasing its temperature. The latter, the result of runoff coming from higher elevations where lakes and rivers are frozen and water temperature is often near to 0 °C in winter. The thicker this brackish surface layer and the greater the difference in density between it and the intermediary layer, the greater the amount of energy needed to mix and disperse this layer (Myksvoll et al., 2014). Heat loss may resultantly be largely confined to the brackish surface layer enabling ice formation during periods of subfreezing temperatures as well as subsequent ice growth. Local knowledge supported by scientific studies highlight the relationship between fresh water flux in winter and ice formation as noted by Green et al. (2004) when examining the impact of hydropower dams on fjords. While seawater temperatures below 0 °C were measured in 2017/18 in Storfjord, in all other fjords and years (see Fig. 14), seawater temperature was several degrees above even the freezing temperature of fresh water on the day of measurement. The 2018/19 season, in particular, displays the possible relationship between a strong gradient in density in the upper water column, a pycnocline, and onset of ice formation. Although warmer than 2017/2018 based on FDDs (see Table 2), runoff is seen to fluctuate through the beginning of December in all fjords with another event occurring at the end of February (Fig. 9). We hypothesize that these events created a fresh/brackish surface layer that led to the formation of ice over a larger area of the fjord when temperatures dropped below freezing (Li and Ingram, 2007).

Once a layer of ice forms, turbulence at the surface that may have initially prevented ice growth will decrease enabling congelation ice growth downward as exemplified by cores gathered in March 2018 where congelation ice dominated (Figs. 11 & 12). Alternatively, a thin layer of ice can provide a platform for snow to accumulate, depressing the surface and leading to flooding of the snowpack and the formation of granular, snow ice once seawater refreezes. The latter is likely the primary process driving the thickening of ice sampled in 2020. In 2019, both mechanisms of growth are clear in the cores with all exhibiting both congelation and granular ice.

4.2. *Conditions at the ice-ocean and ice-air interface and relationship to variations in pore structure*

The proportion of granular to congelation ice is the clearest indicator of different ice conditions in the seven fjords observed (Fig. 12). Through examining bands of different pore structure and density and the associated fluctuations in bulk salinity and $\delta^{18}O$ a more detailed description of how the ice formed may be formulated.

The cores presented in Fig. 10 provide many examples of obvious changes in pore shape, size, and density for example in the congelation ice of the Ramfjord core gathered March 2019. Shown again in Fig. 18 with salinity and $\delta^{18}O$ overlain, pores at 19 cm depth are nearly 2 cm in length and clearly separated then become much smaller and densely packed around 22 cm. Transitions are also apparent at approximately 32 cm and 38 cm with bulk salinity and $\delta^{18}O$ showing clear variation with the two properties at times being negative correlated as at 20 cm depth, or positively correlated as at 35 cm depth. These shifts in pore

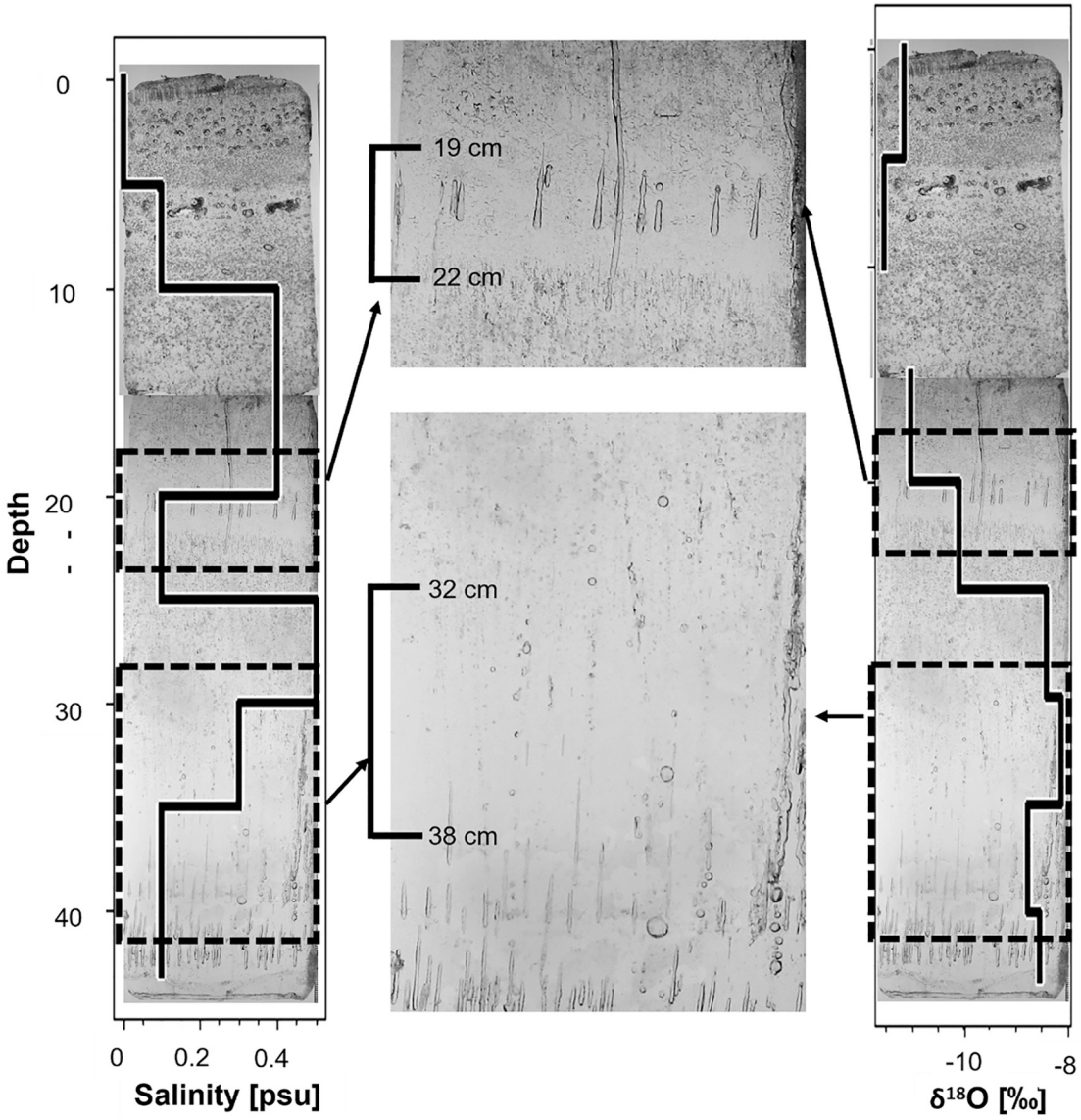

Fig. 18. Backlit thick section of Ramfjord ice core gathered during the 2018/19 season with measurements of bulk salinity and $\delta^{18}O$ overlain with close-up view of two sections.

shape and size, may be caused at least in part to the source of the water, namely the amount of freshwater, in combination with other factors such as ice temperature and growth rate, and flow rate of surface water. Additionally, not all pores will hold liquid brine but be air-filled pores also contributing to the variation in pore characteristics (Light et al., 2003). How these factors combine and the resultant impact on bulk salinity and $\delta^{18}O$ values and ice microstructure are currently poorly understood with further investigation recommended in the specific application of fjord environments.

4.3. The impact of freshwater entry point, fjord geometry, and bathymetry

Multiple cores collected in Beisfjord in 2019 provide an example of how ice conditions may vary along a fjord due to location of freshwater input and pathways it follows. Four cores were gathered along a transect reaching 2.5 km out from the head of the fjord (Fig. 6). In the first two cores, (a) and (b), salinity is similar being <1.0 psu while (a) has lower $\delta^{18}O$ than (b) (see Fig. 13e). This may be due to a difference in growth rate but given the increasing distance from the river, this slight difference might represent a lessening amount of river water at the ice-ocean interface. The third core, (c), has less granular ice (Figs. 10 & 11) but some of the highest values of salinity and $\delta^{18}O$ in the upper 10 cm, gradually decreasing with depth. It is hypothesized that the water that infiltrated the snowpack and refroze in (c) was possibly higher in salinity due to timing or distance from the river. The final core, (d) was composed primarily of nearly transparent ice due to very low porosity (Figs. 10 & 11). In the bottom 8 cm of (c) and the entirety of (d), $\delta^{18}O$ measured between −9.0 to −9.5 ‰. It is hypothesized that the water that led ice at (d) to form from the surface down was also present at the ice-ocean interface of (c), forming the bottom section of this core. The similar decrease in $\delta^{18}O$ found in cores (c) and (d) was not observed in cores (a) and (b). Here, ice had values of $\delta^{18}O$ consistently below 9.0 ‰, often below 10 ‰. The water at the ice-ocean interface at (a) and (b) may therefore have differed from that at (c) and (d) during the period ice was present.

Fjord geometry and bathymetry are also important factors to consider when examining where, when, and what type of ice was present. A constriction, shallow sill, or both can lead to a higher tidal velocity and resultantly heat flux. Significant bends in a fjord's coastline may also act to alter tidal velocity and shelter parts of a fjord from oceanic currents and waves as well as weather patterns, e.g. wind that

blows preferentially from certain directions. In Ramfjord particularly, these bathymetric and coastal features appear to influence the extent of ice. From observation supported by timelapse and satellite imagery, ice formation began at the head of the fjord near the river's entrance and extended out to the sill and abrupt bend soon after initial ice formation in 2019 and 2020. In 2019, ice eventually rounded the corner stopping where a constriction is present. As time progressed, after the day of measurement, the ice pulled back to a similar location as the ice edge observed in 2020 holding more stably before further recession and melt occurred. Further research is recommended to investigate the relationship between ice extent and break-up to coastal geometry and bathymetry.

5. Conclusions

The conditions along coastal Norway may parallel other locations in the Arctic and sub-Arctic regions with similar variability in freshwater flux during the winter months, and weather and oceanic conditions. Along with potentially altering the safety of the ice for access, there are also implications for structures placed in these areas, boats trying to transit through, response to oil spills, as well as the overall health and ecology of fjords and coastal regions. From the work presented here the following conclusions can be drawn:

- De-coupling between the surface and intermediary layer of the fjord plays an important role in ice formation in Norwegian fjords as demonstrated by the distinct difference in ice bulk salinity and $\delta^{18}O$ in the fjord ice versus the fjord water below. This is exemplified by the low values of ice bulk salinity and $\delta^{18}O$ measured, characteristic of ice frozen from fresh water, not seawater.
- The use of freezing degree days may not be a dependable predictor of ice thickness when applied to Norwegian fjords. Substantial consideration must be given to the actual date of onset of ice formation and snow cover. Other factors that may contribute include an influx of warmer water into the fjord and runoff.
- Single-year measurements of ice in Norwegian fjords provide little insight into ice properties one should expect over longer time spans since interannual variability is high.
- Timing is an important factor in ice formation in fjords. How weather and oceanic conditions overlap, including cold weather, runoff, snowfall, wind, tides, and fjord-coast water exchange, will determine when, how much and what type of ice will form.

CRediT authorship contribution statement

Megan O'Sadnick: Conceptualization, Methodology, Software, Validation, Formal analysis, Investigation, Data curation, Writing – original draft, Writing – review & editing, Visualization, Project administration. **Chris Petrich:** Conceptualization, Methodology, Software, Validation, Investigation, Resources, Data curation, Writing – review & editing, Supervision, Project administration, Funding acquisition. **Camilla Brekke:** Conceptualization, Writing – review & editing, Supervision, Funding acquisition. **Jofrid Skarðhamar:** Conceptualization, Methodology, Software, Validation, Formal analysis, Investigation, Resources, Data curation, Writing – review & editing, Supervision. **Øystein Kleven:** Conceptualization, Investigation.

Declaration of Competing Interest

There is no known conflict of interest related to submission of this work to Cold Regions Science and Technology.

Acknowledgements

This work was funded by the Centre for Integrated Remote Sensing and Forecasting for Arctic Operations (CIRFA), a Centre for Research-based Innovation (Research Council of Norway project number 237906), and partners. The authors would also like to thank the two anonymous reviewers and editor, Knut Høyland, who offered many helpful comments to increase the quality of this paper.

References

Anderson, D.L., 1961. Growth rate of sea ice. J. Glaciol. 3 (30), 1170–1172.
Arrigo, K., Mock, T., Lizotte, M., 2010. Primary producers and Sea Ice. In: Thomas, D., Dieckmann, G. (Eds.), Sea Ice, 2nd ed. Wiley-Blackwell, Oxford, pp. 283–326.
Asplin, L., Salvanes, A.G.V., Kristoffersen, J.B., 1999. Nonlocal wind-driven fjord-coast advection and its potential effect on plankton and fish recruitment. Fish. Oceanogr. 8 (4), 255–263. https://doi.org/10.1046/j.1365-2419.1999.00109.x.
Aure, J., Molvær, J., Stigebrandt, A., 1996. Observations of inshore water exchange forced by a fluctuating offshore density field. Mar. Pollut. Bull. 33 (1–6), 112–119.
Bergström, S., 1992. The HBV Model - its Structure and Applications, SMHI Reports RH 4. Swedish Meteorological and Hydrological Institute, Norrköping, p. 4.
Brandon, M., Cottier, F., Nilsen, F., 2010. Sea ice and oceanography. In: Thomas, David N., Dieckmann, G. (Eds.), Sea Ice, 2nd ed. Wiley-Blackwell, Oxford, pp. 79–112.
Cole, D.M., Eicken, H., Frey, K., Shapiro, L.H., 2004. Observations of banding in first-year Arctic Sea ice. J. Geophys. Res. Oceans 109 (C8). https://doi.org/10.1029/2003JC001993.
Cottier, F.R., Nilsen, F., Skogseth, R., Tverberg, V., Skarðhamar, J., Svendsen, H., 2010. Arctic fjords: a review of the oceanographic environment and dominant physical processes. Geol. Soc. Lond., Spec. Publ. 344 (1), 35–50. https://doi.org/10.1144/SP344.4.
Dickens, D., 2011. Behavior of oil spills in ice and implications for Arctic spill response. In: *Proceedings of the Arctic Technology Conference*, Houston, Texas, USA, 7-9 February.
Eicken, H., 1998. Deriving modes and rates of ice growth in the Weddell Sea from microstructural, salinity and stable-isotope data. Antarctic Sea Ice 74, 89–122. https://doi.org/10.1029/ar074p0089.
Eicken, H., Lange, M.A., Wadhams, P., 1994. Characteristics and distribution patterns of snow and meteoric ice in the Weddell Sea and their contribution to the mass balance of sea ice. Ann. Geophys. 12 (1), 80–93. https://doi.org/10.1007/s00585-994-0080-x.
Eicken, H., Dmitrenko, I., Tyshko, K., Darovskikh, A., Dierking, W., Blahak, U., Kassens, H., 2005. Zonation of the Laptev Sea landfast ice cover and its importance in a frozen estuary. Glob. Planet. Chang. 48 (1–3), 55–83. https://doi.org/10.1016/j.gloplacha.2004.12.005.
Eilertsen, H.C., Skarðhamar, J., 2006. Temperatures of north Norwegian fjords and coastal waters: Variability, significance of local processes and air-sea heat exchange. Estuar. Coast. Shelf Sci. 67 (3), 530–538. https://doi.org/10.1016/j.ecss.2005.12.006.
Fofonoff, N., Millard, R., 1983. Algorithms for computation of fundamental properties of seawater. UNESCO Tech. Pap. Mar. Sci. 44.
Gerland, S., Renner, A.H.H., 2007. Sea-ice mass-balance monitoring in an Arctic fjord. Ann. Glaciol. 46, 435–442. https://doi.org/10.3189/172756407782871215.
Gorelick, N., Hancher, M., Dixon, M., Ilyushchenko, S., Thau, D., Moore, R., 2017. Google Earth Engine: Planetary-scale geospatial analysis for everyone. Remote Sens. Environ. 202, 18–27. https://doi.org/10.1016/j.rse.2017.06.031.
Gradinger, R., Friedrich, C., Spindler, M., 1999. Abundance, biomass and composition of the sea ice biota of the Greenland Sea pack ice. Deep-Sea Res. Part II 46 (6–7), 1457–1472. https://doi.org/10.1016/S0967-0645(99)00030-2.
Granskog, M.A., Kaartokallio, H., Shirasawa, K., 2003. Nutrient status of Baltic Sea ice: evidence for control by snow-ice formation, ice permeability, and ice algae. J. Geophys. Res. Oceans 108 (C8). https://doi.org/10.1029/2002JC001386.
Granskog, M.A., Ehn, J., Niemelä, M., 2005a. Characteristics and potential impacts of under-ice river plumes in the seasonally ice-covered Bothnian Bay (Baltic Sea). J. Mar. Syst. 53 (1–4), 187–196. https://doi.org/10.1016/j.jmarsys.2004.06.005.
Granskog, M.A., Kaartokallio, H., Thomas, D.N., Kuosa, H., 2005b. Influence of freshwater inflow on the inorganic nutrient and dissolved organic matter within coastal sea ice and underlying waters in the Gulf of Finland (Baltic Sea). Estuar. Coast. Shelf Sci. 65 (1–2), 109–122. https://doi.org/10.1016/j.ecss.2005.05.011.
Green, J.A.M., Molvaer, J., Stigebrandt, A., 2004. Hydrographic response of Holandsfjord to changed freshwater runoff. J. Geophys. Res. Oceans 109 (C7). https://doi.org/10.1029/2004JC002295.
Holtedahl, H., 1967. Notes on the Formation of Fjords and Fjord-Valleys. Geografiska Annal. Ser. A Phys. Geogr. 49 (2), 188–203.
Hop, H., Wiencke, C., 2019. The ecosystem of Kongsfjorden, Svalbard. In: Hop, H., Wiencke, C. (Eds.), Advances in Polar Ecology. Springer, Cham. https://doi.org/10.1007/978-3-319-46425-1_1.
Hughes, N., 2006. NP57A, NP57B, NP58A, NP58B Norway Pilot. *Sea Ice Conditions: West Coast of Norway from: Lindesnes to Statlandet, Statllandet to Risværfjorden. Offshore and Coastal Waters of Norway from: Risværfjorden to the North Part of Vesterrålen, Andfjorden to Varang*. Argyll, UK: Scottish Association for Marine Science. Engineering under Arctic Conditions, POAC.
Ingram, R.G., Wang, J., Lin, C., Legendre, L., Fortier, L., 1996. Impact of freshwater on a subarctic coastal ecosystem under seasonal sea ice (southeastern Hudson Bay, Canada). I. Interannual variability and predicted global warming influence on river plume dynamics and sea ice. J. Mar. Syst. 7 (2–4), 221–231.
Jeffries, M.O., Shaw, R.A., Morris, K., Veazey, A.L., Krouse, H.R., 1994. Crystal structure, stable isotopes (δ18O), and development of sea ice in the Ross, Amundsen, and

Bellingshausen seas, Antarctica. J. Geophys. Res. Oceans 99, 985–995. https://doi.org/10.1029/93JC02057.
Jones, E.M., Renner, A.H.H., Chierici, M., Wiedmann, I., Lødemel, H.H., Biuw, M., Miller, L.A., 2020. Seasonal dynamics of carbonate chemistry, nutrients and CO2 uptake in a sub-Arctic fjord. Elementa 8. https://doi.org/10.1525/elementa.438.
Kaartokallio, H., Kuosa, H., Thomas, D.N., Granskog, M.A., Kivi, K., 2007. Biomass, composition and activity of organism assemblages along a salinity gradient in sea ice subjected to river discharge in the Baltic Sea. Polar Biol. 30 (2), 183–197. https://doi.org/10.1007/s00300-006-0172-z.
LeGrande, A.N., Schmidt, G.A., 2006. Global gridded data set of the oxygen isotopic composition in seawater. Geophys. Res. Lett. 33 (12).
Li, S.S., Ingram, R.G., 2007. Isopycnal deepening of an under-ice river plume in coastal waters: Field observations and modeling. J. Geophys. Res. Oceans 112 (C7). https://doi.org/10.1029/2006JC003883.
Light, B., Maykut, G.A., Grenfell, T.C., 2003. Effects of temperature on the microstructure of first-year Arctic Sea ice. J. Geophys. Res. 108 (C2), 3051. https://doi.org/10.1029/2001JC000887.
Lussana, C., Saloranta, T., Skaugen, T., Magnusson, J., Tveito, O.E., Andersen, J., 2018. SeNorge2 daily precipitation, an observational gridded dataset over Norway from 1957 to the present day. Earth Syst. Sci. Data 10 (1), 235–249. https://doi.org/10.5194/essd-10-235-2018.
Macdonald, R.W., Paton, D.W., Carmack, E.C., Omstedt, A., 1995. The freshwater budget and under-ice spreading of Mackenzie River water in the Canadian Beaufort Sea based on salinity and 18O/16O measurements in water and ice. J. Geophys. Res. Oceans 100 (C1), 895–919.
Macdonald, R.W., Carmack, E.C., Paton, D.W., 1999. Using the δ18O composition in landfast ice as a record of Arctic estuarine processes. Mar. Chem. 65 (1–2), 3–24.
Mankettikkara, R., 2013. Hydrophysical Characteristics of the Northern Norwegian Coast and Fjords (Doctoral dissertation. Universitetet i Tromsø.
Myksvoll, M.S., Sandvik, A.D., Asplin, L., Sundby, S., 2014. Effects of river regulations on fjord dynamics and retention of coastal cod eggs. ICES J. Mar. Sci. 71 (4), 943–956. https://doi.org/10.1093/icesjms/fst113.
Nan, Y., Tian, F., Hu, H., Wang, L., Zhao, S., 2019. Stable isotope composition of river waters across the world. Water 11 (9), 1760.
Nedbørfelt (REGINE), 2020. Retrieved from. https://www.nve.no/karttjenester/kartdata/vassdragsdata/nedborfelt-regine/.
Nilsen, F., Cottier, F., Skogseth, R., Mattsson, S., 2008. Fjord-shelf exchanges controlled by ice and brine production: the interannual variation of Atlantic Water in Isfjorden, Svalbard. Cont. Shelf Res. 28 (14), 1838–1853. https://doi.org/10.1016/j.csr.2008.04.015.
Oggier, M., Eicken, H., Petrich, C., Wilkinson, J., O'Sadnick, M., 2019. Crude oil migration in sea-ice: Laboratory studies of constraints on oil mobilization and seasonal evolution. Cold Reg. Sci. Technol. 174, 102924.
O'Sadnick, M., Petrich, C., Brekke, C., Skarðhamar, J., 2020. Ice extent in sub-arctic fjords and coastal areas from 2001 to 2019 analyzed from MODIS imagery. Ann. Glaciol. 61 (82), 210–226. https://doi.org/10.1017/aog.2020.34.
Petrich, C., Eicken, H., 2010. Growth, structure, and properties of sea ice. In: Thomas, D., Dieckmann, G. (Eds.), Sea Ice, 2nd ed. Wiley Blackwell, Oxford, pp. 23–77.
Petrich, C., Langhorne, P., Eicken, H., 2011. Modelled Bulk Salinity of growing First-Year. In: Proceedings of the 21st International Conference on Port and Ocean Engineering under Arctic Conditions.
Petrich, C., Karlsson, J., Eicken, H., 2013. Porosity of growing sea ice and potential for oil entrainment. Cold Reg. Sci. Technol. 87, 27–32.
Polashenski, C., Perovich, D., Courville, Z., 2012. The mechanisms of sea ice melt pond formation and evolution. J. Geophys. Res. Oceans 117 (C1). https://doi.org/10.1029/2011JC007231.
Porter, S.C., 1989. Some geological implications of average Quaternary glacial conditions. Quat. Res. 32 (3), 245–261. https://doi.org/10.1016/0033-5894(89)90092-6.
Rikardsen, A.H., Haugland, M., Bjørn, P.A., Finstad, B., Knudsen, R., Dempson, J.B., Holm, M., 2004. Geographical differences in marine feeding of Atlantic salmon post-smolts in Norwegian fjords. J. Fish Biol. 64 (6), 1655–1679. https://doi.org/10.1111/j.0022-1112.2004.00425.x.
Skarðhamar, J., Albretsen, J., Sandvik, A.D., Lien, V.S., Myksvoll, M.S., Johnsen, I.A., Bjørn, P.A., 2018. Modelled salmon lice dispersion and infestation patterns in a sub-arctic fjord. ICES J. Mar. Sci. 75 (5), 1733–1747. https://doi.org/10.1093/icesjms/fsy035.
Skogseth, R., Olivier, L.L., Nilsen, F., Falck, E., Fraser, N., Tverberg, V., Falk-Petersen, S., 2020. Variability and decadal trends in the Isfjorden (Svalbard) ocean climate and circulation – an indicator for climate change in the European Arctic. Prog. Oceanogr. 187, 102394 https://doi.org/10.1016/j.pocean.2020.102394.
Smith, I.J., Langhorne, P.J., Frew, R.D., Vennell, R., Haskell, T.G., 2012. Sea ice growth rates near ice shelves. Cold Reg. Sci. Technol. 83, 57–70.
Stigebrandt, A., 2012. Hydrodynamics and circulation of Fjords. In: Bengtsson, L., Herschy, R.W., Fairbridge, R.W. (Eds.), Encyclopedia of Lakes and Reservoirs. Encyclopedia of Earth Sciences Series. Springer, Dordrecht. https://doi.org/10.5860/choice.50-3613.
Timco, G.W., Weeks, W.F., 2010. A review of the engineering properties of sea ice. Cold Reg. Sci. Technol. 60 (2), 107–129. https://doi.org/10.1016/j.coldregions.2009.10.003.
Tucker, W.B., Perovich, D.K., Gow, A.J., Weeks, W.F., Drinkwater, M.R., 1992. Physical properties of sea ice relevant to remote sensing. Microw. Remote Sens. Sea Ice 68, 9–28.
Turner, K.E., Smith, I.J., Tison, J.L., Verbeke, V., McGuinness, M., Ingham, M., Trodahl, J., 2017. Sea ice growth rates from tide-driven visible banding. J. Geophys. Res. Oceans 122 (6), 4675–4684.
Walker, E., Wiedmann, I., Renner, A., Nikolopoulos, A., Skarðhamar, J., 2021. Pelagic Ecosystem Dynamics between Late Autumn and the Post Spring Bloom in a High Latitute Fjord. Submitted. (In Review).